The GnRH pulse generator activity in mouse models of polycystic ovary syndrome

Ziyue Zhou[1], Su Young Han[1], Maria Pardo-Navarro[1], Ellen G. Wall[1], Reena Desai[2], Szilvia Vas[1], David J. Handelsman[2], Allan E. Herbison[1]

[1]Department of Physiology, Development and Neuroscience, University of Cambridge, Cambridge CB2 3EG, United Kingdom, [2]ANZAC Research Institute, University of Sydney, Sydney, Australia.

Correspondence should be addressed to Allan E. Herbison (email: aeh36@cam.ac.uk)

Disclosures: The authors have nothing to disclose and no competing interests.

Abstract

One in five women worldwide suffer from polycystic ovary syndrome (PCOS) that, alongside subfertility and hyperandrogenism, typically presents with increased luteinizing hormone (LH) pulsatility. As such, it is suspected that the arcuate kisspeptin (ARN^{KISS}) neurons that represent the GnRH pulse generator are dysfunctional in PCOS. We used here *in vivo* GCaMP fiber photometry and other approaches to examine the behavior of the GnRH pulse generator in two mouse models of PCOS. We began with the peripubertal androgen (PPA) mouse model of PCOS but found that it had a reduction in the frequency of ARN^{KISS} neuron synchronization events (SEs) that drive LH pulses. Examining the prenatal androgen (PNA) model of PCOS, we observed highly variable patterns of pulse generator activity with no significant differences detected in ARN^{KISS} neuron SEs, pulsatile LH secretion, or serum testosterone, estradiol, and progesterone concentrations. However, an unsupervised machine learning approach identified that the ARN^{KISS} neurons of acyclic PNA mice continued to exhibit cyclical patterns of activity similar to that of normal mice. The frequency of ARN^{KISS} neuron SEs was significantly increased in algorithm-identified “diestrous stage” PNA mice compared to controls. In addition, ARN^{KISS} neurons exhibited reduced feedback suppression to progesterone in PNA mice and their pituitary gonadotrophs were also less sensitive to GnRH. These observations demonstrate the importance of understanding GnRH pulse generator activity in mouse models of PCOS. The unexpected functional disassociation of cyclical GnRH pulse generator activity in the acyclic PNA mouse indicates

the presence of a complex phenotype with deficits at multiple levels of the hypothalamo-pituitary-gonadal axis.

Introduction

Polycystic ovary syndrome (PCOS) is one of the most common causes of female infertility with variable reproductive and metabolic phenotypes (Bozdag, Mumusoglu et al. 2016, Lizneva, Suturina et al. 2016). Many women with PCOS have an elevated body mass index but up to 30% of patients do not, resulting in PCOS being further classified into obese and lean subtypes (Nestler and Jakubowicz 1997, Kumari, Haq et al. 2005, Toosy, Sodi et al. 2018). Although androgen excess, oligo-menorrhea/anovulation, and the existence of polycystic ovaries are the key diagnostic indicators for PCOS, a common secondary feature is increased luteinizing hormone (LH) pulsatility (Waldstreicher, Santoro et al. 1988, The Rotterdam ESHRE/ASRM-sponsored PCOS consensus workshop group 2004). Basal and pulsatile LH secretion can be up to threefold higher in both lean and obese PCOS women and is considered to be a significant contributor to their subfertility (Morales, Laughlin et al. 1996, Dam, Roelfsema et al. 2002, Phylactou, Clarke et al. 2021). A presumed increase in the frequency of pulsatile gonadotropin-releasing hormone (GnRH) secretion in PCOS women results in an increased LH/follicle-stimulating hormone (FSH) ratio (Wildt, Häusler et al. 1981, Dalkin, Haisenleder et al. 1989). This is thought to drive excess ovarian androgen production that, in turn, impairs estrogen and progesterone feedback regulation of GnRH secretion (Pastor, Griffin-Korf et al. 1998, Chhabra, McCartney et al. 2005, Moore, Prescott et al. 2013, Moore, Prescott et al. 2015).

It has become clear that the arcuate nucleus kisspeptin (ARN^{KISS}) neurons represent the mammalian GnRH pulse generator (Clarkson, Han et al. 2017, Herbison 2018, Goodman, Herbison et al. 2022). These neurons exhibit brief episodes of synchronized activity that release kisspeptin on the distal projections of GnRH neurons to drive pulsatile GnRH secretion into the portal vasculature (Herbison 2021, Liu, Yeo et al. 2021). Recent studies indicate that the synchronized activity amongst ARN^{KISS} neurons required for pulsatile hormone secretion is generated by local glutamatergic transmission that is subsequently modulated by neurokinin B and dynorphin (Qiu, Nestor et al. 2016, Han, Morris et al. 2023, Morris and Herbison 2023). While the ARN^{KISS} neurons are the primary site of estrogen negative feedback suppressing pulsatile GnRH secretion (McQuillan, Clarkson et al. 2022), the mechanism of progesterone feedback remains unclear but could also involve the ARN^{KISS} neurons (Goodman, Holaskova et al. 2011). As such, it is thought that dysfunction within the ARN^{KISS} neuron pulse generator may be responsible for the elevated LH pulse

frequency observed in PCOS (Walters, Gilchrist et al. 2018, Coutinho and Kauffman 2019, Rodriguez Paris and Bertoldo 2019, Ruddenklau and Campbell 2019).

We have developed GCaMP fiber photometry methodologies that allow the activity of the ARN^{KISS} neuron pulse generator to be monitored at high temporal resolution in freely behaving mice (Han, Kane et al. 2019, McQuillan, Han et al. 2019, Vas, Wall et al. 2024). Using this and other approaches, we report here a detailed investigation into the pulse generator activity in two widely used mouse models of PCOS including the peripubertal androgen (PPA) model of “obese PCOS”, and prenatal androgen (PNA) model of “lean PCOS” (Stener-Victorin, Padmanabhan et al. 2020).

Results

Peripubertal androgen (PPA) mice

1. Peripubertal dihydrotestosterone (DHT)-treated animals exhibit significantly increased body weight with acyclic estrous cycles

Female 129S6Sv/Ev C57BL/6 *Kiss1*$^{Cre/+}$,GCaMP6s mice exposed to DHT from 3 weeks of age (PPA: n=4) started to show a significant increase in weight 4 weeks after capsule implantation compared to controls with empty capsules (control: n=5) (Sidak’s multiple comparisons test; Fig.1-Suppl. Fig.1A). The PPA animals were completely acyclic with vaginal cytology only ever showing the diestrous stage (Fig.1-Suppl. Fig.1B-D).

2. Peripubertal exposure to DHT results in a slowed GnRH pulse generator

Abrupt and large increases in arcuate nucleus kisspeptin (ARN^{KISS}) neurons activity, termed synchronization events (SEs), are observed with GCaMP fiber photometry in mice (Clarkson, Han et al. 2017, Han, Kane et al. 2019, McQuillan, Han et al. 2019). Both adult PPA and control mice recorded in diestrus for 24 hours exhibited ARN^{KISS} neuron SEs (Fig.1A,B). The frequency of SEs in PPA mice (n=4) was approximately half that of controls (n=5) with SE frequency/hour showing an inhibitory trend (P = 0.0714, Mann-Whitney U test; Fig.1C) and SE interval significantly increased (P = 0.0159, Mann-Whitney U test; Fig.1D). The SE interval frequency distribution pattern revealed a shift to the right for PPA mice with a tight clustering within the 70-90-minute bin centers (Fig.1E). To compare the dynamics of SEs from control and PPA animals, continuous (10 Hz) photometry recordings were performed in

diestrus to obtain high temporal resolution profiles (Fig.1F). These profiles were the same between control (n=5) and PPA (n=4) animals with SE duration, and both upswing and downswing durations calculated from the full-width half maximum (FWHM) points being not significantly different (Fig.1G-H).

Prenatal androgen (PNA) mice

1. The PNA mouse model exhibits highly disordered estrous cyclicity

Female mice originating from dams treated with DHT on gestational days 16, 17, and 18 were found to have a significantly increased anogenital distance (n=10; $P < 0.001$, Mann-Whitney U test) compared with controls (n=9; Fig.2A). Body weight was not different between PNA and control animals at 10 weeks of age (n=12 per group; $P = 0.6602$, Mann-Whitney U test; Fig.2B). The PNA mice exhibited very disordered estrous cycles remaining mostly in persistent diestrus (71 ± 3%) with occasional excursions to metestrus. The proestrus stage was never encountered and estrus was observed rarely (Fig.2C-E).

2. Circulating gonadal steroid hormone levels are not different between control and PNA animals.

As androgen excess is one of the hallmarks of PCOS, we initially measured serum testosterone levels in control and PNA animals using a commercial testosterone enzyme-linked immunosorbent assay (ELISA) (Risal, Manti et al. 2021). This did not detect any difference in serum testosterone levels between control (n=13) and PNA (n=20) animals in diestrus ($P = 0.8203$, Mann-Whitney U test; Fig.2F). Given concerns over the sensitivity and specificity of the steroid hormone ELISAs (Handelsman, Jimenez et al. 2015), we progressed to using ultrasensitive liquid chromatography-mass spectrometry (LC-MS) (Handelsman, Gibson et al. 2020) to measure the circulating levels of testosterone, androstenedione, estradiol, and progesterone in diestrous PNA and control mice (n=6 per group). No significant differences (Mann-Whitney U tests) were detected for androstenedione, estradiol, or progesterone while all samples were below the limit of detection for testosterone (< 0.01 ng/mL) (Fig.2G-I).

3. Kisspeptin, neurokinin B, and dynorphin immunoreactivity are relatively unchanged within the ARN of PNA mice

Previous studies have found variable effects of PNA treatment on kisspeptin, neurokinin B (NKB), and dynorphin protein and mRNA expression within the ARN (Barnes, Rosenfield et al. , Yan, Yuan et al. 2014, Osuka, Iwase et al. 2016, Gibson, Jaime et al. 2021, McCarthy, Dischino et al. 2021, Moore, Lohr et al. 2021). To re-examine this issue, we assessed levels of immunofluorescence for all three peptides in the ARN of control (n=4-8) and PNA (n=4-6) mice (Fig.2-Suppl. Fig.1A-C). This revealed a significant but modest elevation in kisspeptin immunofluorescence within the rostral ARN (P = 0.0187, Sidak's multiple comparisons test) in PNA mice but not elsewhere in the ARN (Fig.2-Suppl. Fig.1A). No significant changes were detected for NKB or dynorphin immunoreactivity in any region of the ARN (Fig.2-Suppl. Fig.1B,C).

4. PNA animals exhibit highly variable patterns of ARN^{KISS} neuron SEs

Both control and PNA mice exhibited robust SEs across 24-hour recording periods (Fig.3A-D). Control mice recorded in diestrus had approximately 0.8 SEs per hour (Fig.3E) with an SE interval of 74.75 ± 5.71 min (Fig.3F) and a normal-like distribution of SE intervals (Fig.3G). Unexpectedly, diestrous PNA mice exhibited highly variable patterns of ARN^{KISS} neuron activity that could appear similar to diestrous controls (Fig.3C) or very different (Fig.3D) with episodes of multi-peak SEs (mpSEs). However, overall SE frequency and intervals were not different between PNA (n=6) and control (n=7) animals (Fig.3E,F; Mann-Whitney U tests). The frequency distribution of inter-SE intervals in PNA mice exhibited a peak interval cluster around the 10-minute bin center (39%) with a gradual tail off in SE intervals (Fig.3G). Continuous (10 Hz) photometry recordings in diestrus did not reveal any difference in the profiles of single SEs between controls (n=7) and PNA (n=6) animals (Fig.3H-J).

5. PNA mice have elevated mean LH secretion but normal LH pulse frequency

We have previously found a near perfect relationship between ARN^{KISS} neuron SEs and pulsatile LH secretion in male and female mice (Han, Kane et al. 2019, McQuillan, Han et al. 2019). To assess this relationship in PNA mice, ARN^{KISS} neuron recordings were commenced, and tail-tip blood samples taken at 12-minute intervals until an SE was detected after which the blood sampling rate was switched to 6-minute intervals. We observed a perfect correlation between SEs and pulsatile LH secretions in both control and PNA mice: every SE was followed by an LH pulse, and no LH pulses were detected without a preceding SE (Fig.4A,C). Temporal analysis of SEs and LH release indicated that the SE peak precedes each LH peak by 7.7 ± 0.6 minutes and 6.6 ± 0.4 minutes in control (n=7

from 4 mice) and PNA (n=7 from 5 mice) animals (*P* = 0.190, Mann-Whitney U test), respectively (Fig.4B,D).

The absence of significant differences in ARN^{KISS} neuron SE frequency in PNA mice and their tight correlation with pulsatile LH secretion indicated that pulsatile LH secretion may not be different between PNA and control mice. Prior studies have found conflicting data with one finding no difference in LH pulse frequency (McCarthy, Dischino et al. 2021) and another reporting increased LH pulsatility (Moore, Prescott et al. 2015). To re-address this we undertook 4-hour tail-tip blood sampling at 10-minute intervals to assess pulsatile LH secretion in wild-type C57BL6/J diestrous-stage PNA (n=8) and control (n=7) mice. Mean LH levels were found to be significantly elevated in PNA mice (*P* = 0.0205, Mann-Whitney U test; Fig.4E-G) but the variable LH pulse frequency and amplitude were unchanged compared to controls (Fig.4H,I).

To evaluate whether the response of pituitary gonadotrophs to GnRH was altered, PNA and control mice were given GnRH (200 ng/kg, i.p.) at the end of the 4-hour tail-tip bleeding, and two further tail-tip blood samples collected for LH measurement at 10-minute intervals. Both control (n=7) and PNA (n=11) mice showed elevated LH levels in response to exogenous GnRH (Fig.4J). However, PNA mice showed a small but significantly lower level of LH 20 minutes after GnRH injection (P=0.0152, Sidak's multiple comparisons test). The total GnRH-evoked increment in LH release was significantly lower in PNA mice compared to controls (*P* = 0.0028, Mann-Whitney U test, Fig.4K).

6. The pulse generator exhibits cyclical activity in PNA mice

The patterns of ARN^{KISS} neuron SEs recorded from acyclic "diestrous" PNA mice were highly variable and could exhibit typical diestrous-like activity but also characteristics such as mpSEs (Fig.3D) that are only usually observed during estrus and metestrus (Vas, Wall et al. 2024). This suggested that, despite the acyclical state of the PNA mice, the pulse generator may still be undergoing cycles of activity. To assess this, we conducted long-duration photometry recordings in both PNA and control mice for four consecutive days starting on proestrus for controls and any day for the acyclic PNA mice. We have recently found that k-means clustering, an unsupervised machine learning-based approach, provides a very sensitive characterization of ARN^{KISS} neuron activity across the estrous cycle (Vas, Wall et al. 2024). This involves analysis of SEs based on five parameters: the frequency of regular single-peak SEs; the standard deviation of inter-SE intervals for regular SEs; and the number, duration, and profiles of mpSEs (Fig.5A).

All control animals showed typical cycling patterns of ARN^{KISS} neuron activity over the four-day recording period (n=5, two representative examples shown in Fig.5C). The most pronounced features of this cyclicity are the suppression of all SE activity during late proestrus to early estrus (represented by Cluster_0 activity) with a gradual return in SEs during the late estrus (Cluster_1). This is often followed by the appearance of mpSEs (Cluster_3/4) during the estrus to metestrus transition. The activity patterns then become the typical diestrous single SEs with variable frequencies (Cluster_1 & _2) (Fig.5C). Surprisingly, we observed that the ARN^{KISS} neurons in PNA mice also exhibited variable but shifting SE profiles over the four-day recordings despite vaginal smears remaining in metestrus or diestrus throughout (n=4, two examples shown in Fig.5D). These PNA mice exhibited a cyclical pattern of activity similar to that of control mice with a period of slow Cluster_0 activity directly followed by an mpSEs period (Cluster_3/4) and then regular diestrous activity (Cluster_1 & _2) (Fig.5D).

Overall, quantification of the time spent in each cluster pattern over the four days was remarkably similar between control (n=5) and PNA (n=4) mice (Fig.5B). The proportion of Cluster_0 (PNA 21%; control 21%) and Cluster_1 (PNA 44%; control 42%) activity was almost identical with the major trend being a nonsignificant increased time ($P > 0.05$, Sidak's multiple comparisons test) spent in mpSE Cluster_3/4 activity (PNA 20%; control 12%) at the expense of the fast regular SE Cluster_2 pattern (PNA 15%; control 25%) (Fig.5B).

7. *PNA mice have increased diestrous-like GnRH pulse generator frequency*

Given that our earlier recordings from PNA mice (Fig.3C,D) were unavoidably taken from random times of the pulse generator cycle, we used the unsupervised machine learning algorithm above to identify "diestrous-like" (Cluster_1&_2) episodes of ARN^{KISS} neuron SE activity in PNA mice and compared this with diestrous controls. In this case, the frequency of SEs was 48% greater in PNA mice (n=6) compared to control animals (n=7; $P = 0.0029$, Mann-Whitney U test; Fig.6C) as also reflected in a significantly lower inter-SE interval ($P = 0.0047$, Mann-Whitney U test; Fig.6D). The frequency distribution of inter-SE intervals in PNA mice was slightly shifted to the left compared to control mice so that majority of PNA SE intervals were in 10-70 minute bin compared to the 30-90 minute bin centers in control mice (Fig.6E).

8. PNA mice have impaired progesterone negative feedback

Progesterone negative feedback is thought to be abnormal in women with PCOS (Pastor, Griffin-Korf et al. 1998, Chhabra, McCartney et al. 2005) and PNA mice (Moore, Prescott et al. 2015). We assessed the response of ARN^{KISS} neuron activity to vehicle or progesterone (4 mg/kg, i.p.) in PNA and control mice with diestrous activity patterns. As expected (McQuillan, Han et al. 2019), we found a marked suppression of ARN^{KISS} neuron SEs that lasted for up to 6 hours following progesterone in control mice (n=3, $P < 0.001$, Sidak's multiple comparisons test, Fig.7A,B,E). The response in PNA mice was much less consistent, and overall, no significant differences in SE activity detected at any time point (n=3, Fig.7C,D,F).

9. No differences exist in ARN^{KISS} neuron activity in ovariectomized (OVX) PNA and control females

Gonadal steroids play a key role in modulating the activity of the ARN^{KISS} neurons (McQuillan, Han et al. 2019, McQuillan, Clarkson et al. 2022). To assess whether any differences exist in ARN^{KISS} neuron activity in PNA mice in the absence of gonadal steroids, we undertook 24-hour fiber photometry recordings in mice that had been ovariectomized for at least 3 weeks. Removal of gonadal steroids results in increased SE frequency and the emergence of clusters of tightly coupled individual synchronizations as previously described (McQuillan, Clarkson et al. 2022) (Fig.8A,B). We observed no significant differences (Mann-Whitney U tests) between SE frequency (Fig. 8C) or intervals (Fig. 8D,E) in PNA and control animals (n=4 per group). Similarly, high-resolution recordings at 10 Hz did not reveal any differences in SE profiles between OVX control and OVX PNA mice (Fig.8F,H).

Discussion

It is important to establish animal models that faithfully recapitulate the symptoms and features of women with PCOS to be able to make progress in treating the disorder (Stener-Victorin, Padmanabhan et al. 2020). Increased LH pulse frequency is observed in ~75% of women with PCOS and is considered to be a significant contributor to their sub-fertility (Taylor, McCourt et al. 1997). We provide here a detailed assessment of the GnRH pulse generator in two commonly used mouse models of PCOS. The obese PPA mouse model was found to have a pulse generator that actually operates at a slower frequency than normal. In contrast, the PNA mouse model has a pulse generator that is operating faster than normal but, remarkably, maintains cyclical-like patterns of activity despite being in reproductively acyclic mice.

Pulse generator activity in PPA mice

The chronic administration of DHT to female mice from postnatal day 21 generates an androgen receptor-dependent mouse model of PCOS with infertility and metabolic disturbances (Caldwell, Middleton et al. 2014, Caldwell, Edwards et al. 2017, Stener-Victorin, Padmanabhan et al. 2020, Kerbus, Decourt et al. 2024). In agreement with those prior studies, we found that PPA mice start to exhibit increased body weight around four weeks after DHT exposure and are acyclic. Fiber photometry revealed that the frequency of ARN^{KISS} neuron SEs was reduced by ~50% in PPA mice compared to controls. This clearly indicates that the PPA mouse does not provide an appropriate PCOS model of elevated pulse generator activity. Given this, we did not proceed to examine pulsatile LH secretion in PPA mice but note that a recent study has reported pulsatile LH secretion to be unchanged in this animal model (Coyle, Prescott et al. 2022). It is very likely that chronic excess androgen activation in this model provides additional negative feedback suppression of ARN^{KISS} neurons. The treatment of adult OVX female mice with the same DHT regimen is reported to decrease LH pulse frequency and amplitude (Esparza, Terasaka et al. 2020).

Variable reproductive parameters of the PNA mouse model

The PNA mouse model has been studied by many different research groups with some features being identified in a highly consistent manner while others are not (Stener-Victorin, Padmanabhan et al. 2020). Common characteristics, also present in the current study, are those of increased anogenital distance, normal body weight, and highly disrupted estrous cycles (Sullivan and Moenter 2004, Silva, Prescott et al. 2018, Stener-Victorin, Padmanabhan et al. 2020, Gibson, Jaime et al. 2021, McCarthy, Dischino et al. 2021). In contrast, reported differences in circulating gonadal steroid concentrations in PNA mice have been inconsistent among studies. Using ELISAs, some studies have demonstrated PNA mice to have elevated testosterone levels (Sullivan and Moenter 2004, Moore, Prescott et al. 2015, Silva, Prescott et al. 2018) while others (Roland and Moenter 2011), including ourselves now, find no differences. Concerns over the specificity and selectivity of ELISAs for measuring gonadal steroids in mice (Handelsman and Wartofsky 2013, Auchus 2014, Wierman, Auchus et al. 2014, Handelsman, Jimenez et al. 2015) led us to re-assess gonadal steroid hormone levels using gold-standard ultrasensitive LC-MS (Handelsman, Gibson et al. 2020). We previously observed that testosterone levels were usually below the limit of detection in C57/BL6 female mice (Wall, Desai et al. 2023) but considered that any elevated concentrations in PNA mice might become detectable. Unfortunately, this was not

the case, and it remains unclear if testosterone levels are elevated in PNA mice. We were, however, able to detect estradiol and progesterone concentrations and find that neither is different between control and PNA mice. A prior ELISA assessment also reported that estradiol and progesterone levels were unchanged in PNA animals (Moore, Prescott et al. 2015).

Another area of considerable inconsistency among studies involves the effects of PNA treatment on both mRNA and protein expression of kisspeptin, neurokinin B, and dynorphin in the ARN (Yan, Yuan et al. 2014, Osuka, Iwase et al. 2016, Gibson, Jaime et al. 2021, McCarthy, Dischino et al. 2021, Moore, Lohr et al. 2021). We re-investigated this question by quantifying the immunoreactive levels of these three proteins and observed an increase in only kisspeptin expression and only in rostral ARN of PNA animals. While there are important roles for these neuropeptides in modulating ARN^{KISS} neuron synchronizations (Han, Morris et al. 2023, Morris and Herbison 2023) and their subsequent activation of GnRH secretion (Liu, Yeo et al. 2021), these generally inconsistent findings indicate that any PNA-induced changes in the expression of the neuropeptides are subtle. Indeed, the principal determinant of kisspeptin, neurokinin B, and dynorphin expression in ARN^{KISS} neurons is estradiol (Navarro, Gottsch et al. 2009) and we demonstrate here that circulating estradiol levels are not altered in PNA mice.

Pulse generator activity and pulsatile LH in the PNA mouse model

One of the key features of the PNA mouse model is thought to be that of increased pulsatile LH secretion (Stener-Victorin, Padmanabhan et al. 2020). However, this has only been reported in a single study with PNA mice exhibiting an approximately 40% increase in LH pulse frequency (Moore, Prescott et al. 2015). A recent paper undertaking the same tail-tip pulse bleeding approach found that LH pulse frequency was not significantly altered in PNA mice (McCarthy, Dischino et al. 2021). Our present observations may explain these discrepancies. As the pulse generator continues to cycle in the acyclic PNA mouse, it is essentially impossible to define the “pulse generator stage” of a PNA mouse at the time of bleeding and consequently wide variations in LH pulse frequency would be expected. We find here that LH pulse frequency recorded from such random “pulse generator” cycling wild-type PNA mice is not significantly different to that of controls. Nevertheless, with the benefit of being able to measure ARN^{KISS} neuron activity directly, it has been possible to show that “diestrous-stage” PNA mice do have an increased rate of pulse generator frequency compared with controls. As such, the PNA mouse model does to some degree replicate the increased pulse frequency seen in many women with PCOS.

The most striking feature of pulse generator activity in PNA mice is its ability to retain cyclical patterns of activity within a reproductively acyclic mouse. The pulse generator of PNA mice exhibits clear transitions from periods of “estrous-like” Cluster_0 activity through to mpSE-dominated Cluster_3/4 phase and onto regular “diestrous-like” Cluster_1&_2 patterns. The percentage of time PNA mice spend in each pattern of activity was not found to be significantly different to controls. We also note that the dynamics of individual ARN^{KISS} neuron SEs remain unchanged under all conditions in PNA mice, suggesting that the fundamental synchronization mechanism and numbers of contributing neurons is not altered (Han, Morris et al. 2023). This is consistent with the observation that PNA treatment does not alter ARN^{KISS} neuron firing activity in adult acute brain slices (Gibson, Jaime et al. 2021). Together, these observations indicate that the acyclic reproductive phenotype of PNA mice does not result from an absence of cyclical activity in the pulse generator. Equally, a significant impact of PNA treatment on the activity of the GnRH neuron can be excluded (Jaime and Moenter 2022) and, at least in mice, pulse generation occurs autonomously at the GnRH neuron distal dendron with no role for GnRH neuron cell bodies (Wang, Guo et al. 2020, Herbison 2021). The degree to which cyclical GnRH pulse generator activity in PNA mice reflects women with PCOS is unknown. However, a very wide range of LH pulse frequency is found in anovulatory women with PCOS (Taylor, McCourt et al. 1997), suggesting the intriguing possibility that the GnRH pulse generator activity may also continue to cycle in women with PCOS.

Gonadal steroid feedback in PNA mice

Pulse generator activity was found to be identical in ovariectomized PNA and control mice. This indicates that, despite androgen receptors being expressed by ARN^{KISS} neurons in the perinatal period (Watanabe, Fisher et al. 2023), excess DHT exposure at this time does not engender any fundamental differences in their synchronization behavior in the absence of gonads as adults. This suggests that the subtle increase in pulse generator frequency detected here in “diestrous-like” PNA mice arises from the effects of circulating gonadal steroids. As gonadal steroid levels are normal in PNA mice, it is likely that perinatal DHT exposure programs long-term changes in gonadal steroid receptor function in adult PNA mice. While direct estrogen feedback is critical in maintaining the suppressed activity of the pulse generator throughout the estrous cycle (McQuillan, Clarkson et al. 2022), ARN^{KISS} neuron ESR1 expression was not found to be altered in PNA mice (Moore, Lohr et al. 2021).

Reduced progesterone negative feedback is widely considered to be a major factor underlying enhanced LH pulsatility in women with PCOS (Pastor, Griffin-Korf et al. 1998, Chhabra, McCartney et al. 2005) and the ability of progesterone to suppress LH secretion is reduced in OVX PNA mice (Moore, Prescott et al. 2015). Whereas progesterone exerts a robust and prolonged suppression of ARN^{KISS} neuron SEs in normal (McQuillan, Han et al. 2019) and control mice, we find this to be much less effective in PNA females. Precisely how perinatal DHT treatment desensitizes ARN^{KISS} neurons to progesterone is unknown and could occur directly or indirectly (Moore, Lohr et al. 2021). Reported effects of PNA on progesterone receptors in the ARN are inconsistent with studies reporting either reduced or unchanged expression (Moore, Prescott et al. 2015, Gibson, Jaime et al. 2021, Moore, Lohr et al. 2021), although one recent study found a 30% reduction in progesterone receptor mRNA expression by ARN^{KISS} neuron in PNA mice (Moore, Lohr et al. 2021).

Although we find that the PNA mouse has reduced progesterone feedback at the level of the pulse generator, as is suspected for women with PCOS, it is unclear how this might pattern ARN^{KISS} neuron activity. Control and PNA mice exhibit similar proportions of time with halted or slow pulse generator activity (Cluster_0). This pattern of activity is thought to occur in response to increased progesterone level following the LH surge (McQuillan, Han et al. 2019, Vas, Wall et al. 2024). Thus, it is somewhat perplexing to find clear Cluster_0 activity in PNA mice that have reduced sensitivity to progesterone negative feedback. This might suggest that in other mechanisms can become responsible for luteal phase slowing of pulse generator activity in PNA mice. Equally, is unclear how reduced progesterone feedback could elevate the “diestrous-like” pattern of ARN^{KISS} neuron activity, although roles for progesterone outside the luteal phase have been suggested (Leipheimer, Bona-Gallo et al. 1984).

Previous studies have demonstrated that the estrogen-activated LH surge mechanism is normal in PNA mice (Moore, Prescott et al. 2013) and, despite proestrous smears never being observed in PNA mice, copra lutea can be found suggesting that LH surges and ovulation can occur (Moore, Prescott et al. 2013, Lei, Ding et al. 2017, McCarthy, Dischino et al. 2021). This raises the intriguing possibility that the GnRH surge generator may also be operational in PNA mice but masked by abnormal downstream signalling. In that regard, we note that pituitary gonadotroph sensitivity to GnRH is blunted in PNA mice as previously reported (Silva, Desroziers et al. 2019). Given that pulse generator activity is the same in ovariectomized PNA and control mice, reduced gonadotroph sensitivity would explain the reduced rise in LH following ovariectomy in PNA mice observed in other studies (Moore, Prescott et al. 2013, Moore, Prescott et al. 2015). Nevertheless, we note that the PNA

mouse clearly does not model women with PCOS that show a much-elevated LH response to GnRH (Barnes, Rosenfield et al. 1989, Batrinos 1993, Morales, Laughlin et al. 1996, Patel, Coffler et al. 2003)

In summary, we report here that the GnRH pulse generator operates at a lower frequency in PPA mice, but at a higher frequency when “diestrous-like” pulse generator activity was analyzed in PNA mice. From the perspective of understanding enhanced pulsatile LH secretion in women with PCOS, the PNA model is clearly the most appropriate model. However, we note that many features of PNA mice such as their pulse generator free-running behavior in the ovariectomized state and gonadal steroid hormone concentrations are normal. Remarkably, we find evidence that the pulse generator continues to exhibit estrous cycle-like patterns of activity within an acyclic PNA mouse model. Thus, the anovulatory phenotype of PNA mice arises in a complex manner from deficits likely at many levels of the hypothalamo-pituitary-ovarian axis. The degree to which the PNA mouse model reflects women with PCOS remains an important, albeit very difficult, question to address.

Methods

Mice

Female 129S6Sv/Ev C57BL/6 *Kiss1*$^{Cre/+}$mice (Yeo, Kyle et al. 2016) were crossed with the Ai162 (TIT2L-GC6s-ICL-tTA2)-D Cre-dependent GCaMP6s males (JAX stock #031562) (Daigle, Madisen et al. 2018) to generate *Kiss1*-Cre/+,*Ai126D* mice as previously characterized (Han, Morris et al. 2023). Mice were group-housed in conventional cages with environmental enrichment under conditions of controlled temperature (22 ± 2 ^{0}C) and lighting (12-hour light/12-hour dark cycle; lights on at 05:30 or 07:00) with *ad libitum* access to food (RM3 (E), Special Diets Services, UK) and water. All animal experimental protocols were approved by the University of Cambridge, UK (P174441DE). Where required, mice were bilaterally ovariectomized (OVX) under isoflurane anesthesia at least 3 weeks prior to experimentation.

Peripubertal androgen (PPA) model

Peripubertal female mice were exposed to DHT as previously described (van Houten, Kramer et al. 2012, Caldwell, Edwards et al. 2017). Briefly, peripubertal female mice (21-23 days old) were implanted subcutaneously (s.c.) with either an empty (control) or

dihydrotestosterone (DHT)-filled (PPA) 1-cm silastic implants (id, 1.47 mm; od, 1.95 mm, Dow Corning Corp, catalog no. 508–006). These silastic implants containing ~10 mg DHT provide steady-state DHT release for at least 6 months (Singh, O'Neill et al. 1995). The body weight of these animals was monitored weekly until optic fiber implantation at the 10 weeks of age.

Prenatal androgen (PNA) model

Adult females were paired with males and checked for copulatory plugs, indicating day 1 of gestation. Pregnant dams were given s.c. injections of sesame oil vehicle (100 µL) alone or containing 250 µg of DHT on gestational days 16, 17, and 18 (Sullivan and Moenter 2004). Female offspring from androgen-treated (PNA) and vehicle-treated (control) dams were used for experiments.

Estrous cycle determination

The estrous cycle stage was determined by the relative ratio of leukocytes, cornified, and nucleated cells observed in the vaginal epithelial cell smear samples on the morning of collection (Ajayi and Akhigbe 2020). The smears were collected using 5 µL of sterile phosphate-buffered saline (PBS) which was transferred to a glass slide to air dry before staining with filtered Giemsa (1:1 in MilliQ water) and examined under a light microscope.

Testosterone ELISA measurements and analysis

Blood samples for testosterone measurement were collected in the afternoon of diestrus through a tail-tip blood sample prior to ovariectomy or from the inferior vena cava before perfusion. The samples were then spun at room temperature at 3,000 rpm for 10 minutes. Serum was collected and kept at –20°C until the day of hormone measurement. Serum testosterone levels were measured using the testosterone rat/mouse ELISA kit according to the manufacturer’s instructions (Demeditec Diagnostics, GmbH, DEV9911, Kiel, Bermany). The assay sensitivity for mouse testosterone ELISA was 0.066 ng/mL, and intra-assay coefficient of variation was 6.5%.

Liquid Chromatography–Mass Spectrometry (LC-MS)

Terminal blood samples were collected from the inferior vena cava of anaesthetized control and PNA animals at 10:00 on diestrus exactly as described previously (Wall, Desai et al.

2023). Plasma levels of estradiol, progesterone, testosterone, and androstenedione were measured using liquid chromatography-mass spectrometry (LC-MS) (Handelsman, Gibson et al. 2020).

Quantification of kisspeptin/neurokinin B/dynorphin expression in ARN

Adult diestrous PNA and control female mice were given a lethal dose of pentobarbital (3 mg/100µL, intraperitoneal, i.p.) and perfused transcardially with 4% paraformaldehyde (PFA). Brains were post-fixed in 4% PFA for 1 hour at 4°C and transferred to 30% sucrose at 4°C until sunk. Forty-µm-thick sections were collected with microtomes and processed for kisspeptin and neurokinin B (NKB) immunofluorescence and dynorphin (DYN) Nickel-3,3′-Diaminobenzidine (DAB) staining. For kisspeptin staining, brain sections were incubated with rabbit anti-kisspeptin (1:5,000, AC566; a gift from Dr. Alain Caraty) followed by goat anti-rabbit Alexa Fluor 568 (1:500, Molecular Probes). For NKB staining, brain sections were incubated with guinea pig anti-NKB (1:5,000, IS-3/61, a gift from Dr. Philippe Ciofi) followed by biotinylated goat anti-guinea pig IgG (1:1,000, Vector Laboratories) and DyLight Streptavidin 488 (1:500, BioLegend). Images were taken using a Leica SP8 Laser Scanning Confocal Microscope (Leica Microsystems) at the Cambridge Advanced Imaging Center and analyzed using ImageJ. Brain sections for DYN Nickel DAB labeling were incubated with rabbit anti-DYN B (1:12,000, a gift from Dr. Philippe Ciofi) (Griffond, Deray et al. 1993) followed by biotinylated goat anti-rabbit IgG (1:200, Vector Laboratories). Brain sections were further incubated in avidin-biotin peroxidase solution before reacting with Nickel DAB developing solution. Images were taken using an Olympus BX43 upright microscope with DP74 digital camera (Olympus Life Science) and analyzed using Image J.

Stereotaxic surgery and GCaMP fiber photometry

Adult female PNA, PPA, and their respective control *Kiss1*-Cre/+,*Ai126D* mice (10-14 weeks old) were anesthetized with 2% isoflurane, given meloxicam (5 mg/kg, s.c.), buprenorphine (0.05 mg/kg, s.c.), and dexamethasone (10 mg/kg, s.c.) and placed in a stereotaxic apparatus. A small hole was drilled in the skull and a unilateral indwelling optical fiber (400 µm diameter; 0.48 NA, Doric LenSEs, Quebec, Canada) was implanted directly above the mid-caudal ARN (2.0 mm posterior to bregma, 3.0 mm lateral to the superior sagittal sinus, 5.93 mm deep). Following optic fiber implantation, mice were monitored through recovery for 5 days and received post-operative analgesics (meloxicam, 5 mg/kg; orally) for up to two days. Then mice were handled daily for at least 3 weeks and habituated to the fiber

photometry recording setup before fluorescence signals were recorded from freely behaving mice in their home cages.

Fiber photometry was undertaken as detailed previously (Clarkson, Han et al. 2017). Photometry systems were built using Doric components (Doric Lenses, QC, Canada) and National Instrument data acquisition board (TX, USA) based on a previous design (Lerner, Shilyansky et al. 2015). Blue (465-490 nm) and violet (405 nm) LED lights were sinusoidally modulated at frequencies of 531 and 211 Hz respectively. Both lights were focused onto a single fiber optic connected to the mouse. The light intensity at the tip of the fiber was 30-80 micro watts. Emitted fluorescence signal from the brain was collected via the same fiber, passed through a 500-550 nm emission filter, before focused onto a fluorescence detector (Doric, QC, Canada). The emissions were collected at 10 Hz and the two GCaMP6 emissions were recovered by demodulating the 465-490 nm signals (calcium-dependent) and 405 nm (calcium independent) signals.

Fluorescence signals were sampled using either a scheduled mode (5/15 seconds on/off) or a continuous mode of light emission with custom software (Tussock Innovation). Twenty-four-hour recordings were made from PNA, PPA, and their respective control female mice in the diestrous stage starting 4 hours after lights-on. Four-day recordings were started on proestrus for control mice and on any diestrous or metestrous stage for PNA mice. Continuous data acquisition mode was used to provide high temporal resolution comparisons of SEs. Signals from each SE were normalized to its peak (intact: -120 to +120 seconds; OVX: -120 to +200 seconds from the peak time). The full widths at half maximum (FHWM) of SE were determined at half-maximal amplitude of the normalized SEs. Averaged SE parameters for each animal were calculated before computing the means for each treatment group.

Analysis was performed in MATLAB with the subtraction of 405 signal from 465-490 signal to extract the calcium-dependent fluorescence signal. An exponential fit algorithm was used to correct for baseline shift. The signal was calculated in dF/F (%) with the equation $dF/F = (F_{fluorescence}-F_{baseline})/ F_{baseline}) \times 100$. The Findpeaks algorithm was used to detect SEs with peaks in dF/F greater than 50% of the maximum signal in each recording. Inter-SE intervals represent the time between peak values of each SEs. Multi-peak SE in PNA animals and cluster SE in OVX were analyzed as one SE and SE intervals were calculated from the first peak.

Serial blood sampling, GnRH injection, and LH measurement

Mice were handled daily for at least 3 weeks to habituate for tail-tip bleeding. To examine the relationship between ARN^{KISS} neuron SEs and pulsatile LH secretion, freely behaving mice were attached to the fiber photometry system, and 4 µL blood samples were taken every 6 or 12 min from the tail-tip over a period of 2 to 4 hours during recording. For standard serial blood sampling experiments, LH secretion was measured by obtaining 4 µL blood samples every 10 minutes for 4 hours (between 12:00 and 17:00). At the end of the bleeding period, 200 ng/kg body weight of GnRH (Bachem, catalog No. 4033013, Switzerland) was injected i.p., and two more blood samples were collected at 10-minute intervals. Whole blood samples were diluted 1:15 in 1x PBS with 0.05% Tween 20 (PBS-T) for LH ELISA (Steyn, Wan et al. 2013), an assay sensitivity of 0.04 ng/mL, as well as intra-assay and interassay coefficients of variation of 9.3% and 10.5%, respectively. Pulses were defined and analyzed by PULSAR with the settings optimized for intact female mice: G1 = 3.5, G2 = 2.6, G3 = 1.9, G4 = 1.5, and G5 = 1.2 (Porteous, Haden et al. 2021).

K-means clustering

Data analysis and unsupervised k-means clustering analysis were performed without vaginal cytology information as previously described (Vas, Wall et al. 2024). Synchronization events with multiple peaks occurring within 160s were defined as mpSEs. In brief, 4-day recordings were segmented into 24-hour periods before applying a customized MATLAB code to extract features of the population activity of the ARN^{KISS} neurons including the (i) number of SEs within a given time period; (ii) prevalence of different type of SEs (single- and mpSEs); (iii) inter-SE intervals, variation in the inter-SE intervals (reflecting regularity of activity patterns); and (iv) shape of the SEs (height, variation in height, half-duration). These 24-hour periods were further fragmented using a 7-hour window size with 1-hour sliding steps. The first and the last 3 hours of each 24-hour recording were extrapolated from the assignment of the 4th and 21st hours, respectively. The following parameters were used to describe the activity pattern of ARN^{KISS} neurons: (i) number of SEs, where mpSEs were counted as a single SE; (ii) standard deviation (SD) of inter-SE intervals; (iii) number of mpSEs; (iv) average number of peaks within an mpSEs; and (v) average duration of mpSEs. All these parameter values were then linearly rescaled to values between 0 and 1. To perform k-means clustering on the data set, we used RapidMiner Studio's (https://rapidminer.com, educational license) built-in module (k = 5, number of runs with random initiations = 100, measure types = "NumericalMeasures", numerical measure = "EuclideanDistance", max optimization steps = 100). Cluster centroid data and cluster labels (to each 7-hour time window) were exported

from RapidMiner Studio and were visualized in R (using “ggplot2”, “readr” and “fmsb” libraries).

Progesterone injection

Progesterone stock solution (800 µg/mL) was prepared by dissolving 8 mg of progesterone (Sigma, Catalog No. P0130) in 1 mL ethanol followed by 1:10 dilution in sesame oil. Diestrous female mice were recorded for 3 hours before an i.p. injection of progesterone (4 mg/kg body weight) or vehicle (100 µL, sesame oil). A previous study has shown that i.p. injection of progesterone at 8 mg/kg body weight to C57BL/6 mice results in peak circulating progesterone concentrations of 110 ng/mL before dropping to 34 ng/mL 1 hour later (Wong, Ray et al. 2012). Circulating progesterone levels at proestrus in C57BL/6 mice are 22 ± 4 ng/mL (Wall, Desai et al. 2023), so we employed half of this dose to test the sensitivity of progesterone negative feedback to ARN^{KISS} neurons.

Statistical analysis

All statistical analyses were performed using GraphPad Prism 10 software. Depending on different experimental designs, and the nature of data distribution, data were analyzed by Mann-Whitney U tests, Kruskal-Wallis test followed by Dunn’s multiple comparison tests, two-way ANOVA followed by Sidak’s multiple comparisons test, or two-way repeated-measures ANOVA followed by Sidak’s multiple comparisons test. The threshold level for statistical significance was set at $P < 0.05$ with data presented as mean ± SEM with each dot representing one animal.

Acknowledgement

This research was supported by the Wellcome Trust (212242/Z/18/Z) to AEH and Medical Research Council (MR N013433-1) and Harding Distinguished Postgraduate Scholars Programme Leverage Scheme to ZZ.

Figures legends

Figure 1 – figure supplement 1. ***Peripubertal androgen (PPA) treatment causes an increase in body weight and a loss of estrous cyclicity.***

(A) Weekly body weight of animals (mean ± SEM) with blank (control: n=5) or dihydrotestosterone (PPA: n=4) capsules. Asterisks above each weekly data point denote significance from Sidak's multiple comparisons test. Asterisks between lines denote the mean effect of the capsule over 7 weeks. Two-way repeated-measure ANOVA with Sidak's multiple comparisons test. **(B)** The proportion of time spent at each stage of the estrous cycle over 21 days (n=4-5 per group). Two-way ANOVA followed by Sidak's multiple comparisons tests. **(C-D)** Representative graphs of estrous cycle pattern over 21 days in **(C)** control and **(D)** PPA females. P, proestrus; E, estrus; M, metestrus; D, diestrus. Data show mean ± SEM. Each circle is an individual animal. * $P < 0.05$, ** $P < 0.01$, *** $P < 0.001$.

Figure 1. ***Slower pulse generator activity in PPA animals.***

Representative 24-hour photometry recordings showing synchronization events (SEs) observed in diestrous (**A**) control and (**B**) PPA females with the light-off period (19:00-07:00) represented by the shaded area and expanded views of the traces (13:00-17:00) from (A-B). Triangles point to identified SEs. (**C**) SE frequency and (**D**) SE intervals in control (n=5) and PPA (n=4) mice. Mann-Whitney U tests. (**E**) Frequency histograms showing relative SE frequencies occurring in 20-minute bins, calculated separately for controls (white, n=114, 5 mice) and PPA (orange, n=55, 4 mice). X-axis represents the bin centers. (**F**) Continuous recordings at 10 Hz sampling rate showing normalized profile of SE overlaid from control (black, 7 SEs from 5 animals) and PPA (orange, 5 SEs from 4 animals). 'a' and 'b' give values of full width at half maximum (FWHM) upswing and downswing respectively. (**G**) FWHM length of control (n=5) and PPA (n=4) animals. Mann-Whitney U test. (**H**) Durations of upswing and downswing for control (n=5) and PPA (n=4) animals, respectively. Kruskal-Wallis test followed by Dunn's multiple comparisons test. Data show mean ± SEM. Each circle is an individual animal. * $P < 0.05$

Figure 2. ***Prenatal androgen exposure leads to increased anogenital distance and disrupted estrous cyclicity.***

(**A**) Anogenital distance (control: n=9; PNA: n=10) and (**B**) Body weight of control and PNA animals (n=12 per group). Mann-Whitney U tests. (**C**) Proportion of time spent at each estrous cycle stage over 21 days (n=7 per group). Two-way ANOVA followed by Sidak's post-hoc tests. (**D-E**) Representative graphs of estrous cycle pattern in (**D**) control and (**E**) PNA females. P, proestrus; E, estrus; M, metestrus; D, diestrus. (**F**) Serum testosterone level of control (n=13) and PNA (n=20) animals in diestrus measured by enzyme-linked immunosorbent assay (ELISA). The limit of detection for testosterone ELISA is 0.066 ng/mL. (**G-I**) Plasma levels of (**G**) androstenedione, (**H**) estradiol, and (**I**) progesterone in control and PNA animals measured using liquid chromatography-mass spectrometry (LC-MS). Blood

samples were collected at 10:00 diestrus (n=6 per group). Dotted lines represent the limit of detection for each hormone. Androstenedione: 0.05 ng/mL; estradiol: 0.50 pg/mL; progesterone: 0.05 ng/mL. All samples were below limit of detection for testosterone LC-MS measurement (< 0.01 ng/mL). Mann-Whitney U tests. Data show mean ± SEM. Each circle is an individual animal. ** P < 0.01, *** P < 0.001.

Figure 2 – figure supplement 1. ***Slightly increased kisspeptin immunofluorescence in the rostral arcuate nucleus of PNA mice.***

Representative arcuate nucleus images of (**A**) Kisspeptin (KISS), (**B**) Neurokinin B (NKB) immunofluorescent staining, and (**C**) Dynorphin (DYN) Nickel-3,3′-Diaminobenzidine (DAB) staining from control and PNA animals, along with the quantified immunoreactive level in rostral, middle, and caudal arcuate nucleus (rARN, mARN, cARN) in control (n=4-8) and PNA (n=4-6) animals. Scale bars represents 100 µm. Two-way ANOVA followed by Sidak's multiple comparisons test. Data show mean ± SEM. Each circle is an individual animal. Asterisk represents significant multiple comparisons results. * *P* < 0.05

Figure 3. ***PNA animals exhibit highly variable patterns of ARN^{KISS} neuron SEs***

Representative 24-hour photometry recordings showing SEs observed in (**A,B**) two control and (**C,D**) two PNA females with the light-off period (17:30-05:30 or 19:00-07:00) represented by the shaded area. Recordings were performed when vaginal cytology indicated diestrus. (**E**) SE frequency and (**F**) SE intervals in control (n=7) and PNA (n=6) mice. Mann-Whitney U tests. (**G**) Frequency histograms showing relative SE frequencies occurring in 20-minute bins, calculated separately for controls (black, n=123, 7 mice) and PNA (red, n=98, 6 mice). X-axis represents the bin centers. Multi-peak SE (mpSE) with peaks occurring within 160 seconds was considered as one SE with interval calculated from the first peak. (**H**) Continuous (10 Hz) recording showing normalized mean profile of SE overlaid from control (black, 22 SEs from 7 animals) and PNA (red, 20 SEs from 6 animals). (**I**) FWHM length (upswing + downswing) in control (n=7) and PNA (n=6) animals. Mann-Whitney U test. (**J**) Durations of FWHM upswing and downswing for control (n=7) and PNA (n=6) animals, respectively. Kruskal-Wallis test followed by Dunn's multiple comparisons test. Data show mean ± SEM. Each circle is an individual animal.

Figure 4. ***Increased total LH concentration but normal LH pulse frequency in PNA animals.***

Representative examples from (**A**) control and (**C**) PNA mice showing the relationship of SEs (black) with LH secretions (red). Triangles and red asterisks indicate identified SEs and LH pulses, respectively. Normalized increase in LH plotted against the SEs in (**B**) control

and (**D**) PNA animals. The amplitudes of SEs and serum LH levels were normalized to their peaks, with time 0 being the peak of LH in control (n=7 from 4 mice) and PNA (n=7 from 5 mice) animals. Representative examples of LH pulse profiles in (**E**) control and (**F**) PNA animals. Red asterisks indicate identified LH pulses. (**G**) Total LH concentration, (**H**) LH pulse frequency per hour, and (**I**) LH pulse amplitude in diestrous control (n=7, with 13 LH pulses) and PNA (n=8, with 21 LH pulses) mice during 4-hour sampling at 10-minute intervals. Mann-Whitney U tests. (**J**) Change in LH levels following an intraperitoneal injection of GnRH (200 ng/kg, i.p.) in diestrous control (n=7) and PNA (n=11) mice. An asterisk above the 20 minutes data point denote significance between LH levels in control and PNA from two-way repeated-measure ANOVA followed by Sidak's post-hoc tests. (**K**) GnRH-evoked changes in LH levels in control (n=7) and PNA (n=11) mice were calculated by the difference in LH levels before (-10 minutes and 0 minutes) and after (10 minutes and 20 minutes) GnRH injections. Mann-Whitney U test. Data show mean ± SEM. Each circle is an individual animal. * $P < 0.05$, ** $P < 0.01$

Figure 5. ***PNA animals exhibit cycling pulse generator activity.***

(**A**). Cluster centroid values for normalized parameters used in k-means clustering with a schematic plot of corresponding photometry recordings patterns. The parameters used for cluster assignments are labelled in Cluster_0 with the following axes: (top) standard deviation (SD) of SE intervals, (top right) number of multi-peak SEs (mpSEs), (bottom right) number of single SEs, (bottom left) number of peaks in mpSEs, (top left) duration of mpSEs. All axes have a minimum value of 0 and maximum value of 1. (**B**) Bar graph indicating proportion of the cluster-assignments for 4-day recordings in control (n=5) and PNA (n=4) animals. Data show mean ± SEM. (**C-D**) Representative examples of four-day consecutive recording of ARN^{KISS} activity and corresponding hourly k-means cluster assignments in (**C**) two control animals starting in proestrus on day 1 and transiting to diestrus on day 4 according to vaginal smears; (**D**) two PNA animals remaining in either metestrus or diestrus for four days. Light-off periods (19:00-07:00) are represented by the shaded area in the photometry recording. Color fields represent the assigned clusters for the center (4th hour) of the 7-hour moving time windows. Estrous stages of the mice determined by vaginal lavage at the beginning and the end of each 24-hour recording were labelled above the corresponding k-means cluster assignments: proestrus to estrus (PE), estrus to metestrus (EM), metestrus to diestrus (MD), stuck in metestrus (MM), or stuck in diestrus (DD). K-means clustering was performed without vaginal cytology information.

Figure 6. ***Faster ARN^{KISS} neuron synchronization events in "diestrous-like" PNA animals.***

Representative 24-hour photometry recordings showing ARN^{KISS} neuron SEs observed in (**A**) diestrous control and (**B**) algorithm-identified diestrous PNA females. The light-off period (17:30-05:30) is represented by the shaded area. (**C**) SE frequency and (**D**) SE intervals in control (n=7) and PNA (n=6) mice. Mann-Whitney U tests. (**E**) Histogram showing percentage of SE interval frequencies occurring in 20-minute bins, calculated separately for controls (black, n=119, 7 mice) and PNA (red, n=151, 6 mice) animals. X-axis represents the bin centers.

Figure 7. ***Defective progesterone negative feedback in PNA animals****.*

(**A-D**) Examples of 15-hour photometry recordings of the pulse generator activity in (**A-B**) control and (**C-D**) PNA animals receiving (**A**,**C**) vehicle (Veh) or (**B**,**D**) progesterone (P4, 4 mg/kg) i.p. injections. Dashed line represents when i.p. injection took place. Normalized number of SEs in (**E**) control (n=3) and (**F**) PNA (n=3) animals before and after vehicle (black) and P4 (red) injections. Data were analyzed in 3-hour bins and normalized to the number of SEs before injections (-3-0 h) for each mouse. The asterisks above the data point denote significant effects at indicated time periods compared to the pre-treatment period (-3-0 h) by Sidak's multiple comparisons test. Data represent mean ± SEM. Two-way repeated-measure ANOVA with Sidak's multiple comparisons tests. *** $P < 0.001$.

Figure 8. ***Similar ARN^{KISS} activity and SE profiles in control and PNA animals following ovariectomy.***

Representative 24-hour photometry recordings showing ARN^{KISS} neuron SEs observed in (**A**) control and (**B**) PNA females 3 weeks after ovariectomy (OVX) with the light-off period (19:00-07:00) represented by the shaded area and expanded views of the traces (13:00-15:00) from (A-B). (**C**) SE frequency and (**D**) SE intervals in control and PNA mice (n=4), Mann-Whitney U tests. (**E**) Histogram showing relative SE frequencies occurring in 5-minute bins, calculated separately for controls (n=212, 4 mice) and PNA (n=233, 4 mice) animals. X-axis represents the bin centers. Each SE cluster was analyzed as a single SE with the interval calculated from the first peak. (**F**) Continuous recordings at 10 Hz sampling rate showing normalized profile of SEs following OVX overlaid from control (black, 14 SEs from 4 animals) and PNA (red, 10 SEs from 4 animals). (**G**) FWHM length of OVX control and PNA animals (n=4). Mann-Whitney U test. (**H**) Durations of upswing and downswing for control and PNA animals (n=4), respectively. $P > 0.05$, Kruskal-Wallis test followed by Dunn's multiple comparisons test. Data show mean ± SEM. Each circle is an individual animal.

References

Ajayi, A. F. and R. E. Akhigbe (2020). "Staging of the estrous cycle and induction of estrus in experimental rodents: an update." Fertil Res Pract **6**: 5.

Auchus, R. J. (2014). "Steroid assays and endocrinology: best practices for basic scientists." Endocrinology **155**(6): 2049-2051.

Barnes, R. B., R. L. Rosenfield, S. Burstein and D. A. Ehrmann (1989). "Pituitary-ovarian responses to nafarelin testing in the polycystic ovary syndrome." N Engl J Med **320**(9): 559-565.

Barnes, R. B., R. L. Rosenfield, S. Burstein and D. A. Ehrmann (1989). "Pituitary-Ovarian Responses to Nafarelin Testing in the Polycystic Ovary Syndrome." New England Journal of Medicine **320**(9): 559-565.

Batrinos, M. L. (1993). "Diagnostic Dilemmas in Polycystic Ovarian Syndrome." Annals of the New York Academy of Sciences **687**(1): 230-234.

Bozdag, G., S. Mumusoglu, D. Zengin, E. Karabulut and B. O. Yildiz (2016). "The prevalence and phenotypic features of polycystic ovary syndrome: a systematic review and meta-analysis." Human Reproduction **31**(12): 2841-2855.

Caldwell, A. S., L. J. Middleton, M. Jimenez, R. Desai, A. C. McMahon, C. M. Allan, D. J. Handelsman and K. A. Walters (2014). "Characterization of reproductive, metabolic, and endocrine features of polycystic ovary syndrome in female hyperandrogenic mouse models." Endocrinology **155**(8): 3146-3159.

Caldwell, A. S. L., M. C. Edwards, R. Desai, M. Jimenez, R. B. Gilchrist, D. J. Handelsman and K. A. Walters (2017). "Neuroendocrine androgen action is a key extraovarian mediator in the development of polycystic ovary syndrome." Proc Natl Acad Sci U S A **114**(16): E3334-e3343.

Chhabra, S., C. R. McCartney, R. Y. Yoo, C. A. Eagleson, R. J. Chang and J. C. Marshall (2005). "Progesterone Inhibition of the Hypothalamic Gonadotropin-Releasing Hormone Pulse Generator: Evidence for Varied Effects in Hyperandrogenemic Adolescent Girls." The Journal of Clinical Endocrinology & Metabolism **90**(5): 2810-2815.

Clarkson, J., S. Y. Han, R. Piet, T. McLennan, G. M. Kane, J. Ng, R. W. Porteous, J. S. Kim, W. H. Colledge, K. J. Iremonger and A. E. Herbison (2017). "Definition of the hypothalamic GnRH pulse generator in mice." Proc Natl Acad Sci U S A **114**(47): E10216-e10223.

Coutinho, E. A. and A. S. Kauffman (2019). "The Role of the Brain in the Pathogenesis and Physiology of Polycystic Ovary Syndrome (PCOS)." Med Sci (Basel) **7**(8).

Coyle, C. S., M. Prescott, D. J. Handelsman, K. A. Walters and R. E. Campbell (2022). "Chronic androgen excess in female mice does not impact luteinizing hormone pulse frequency or putative GABAergic inputs to GnRH neurons." Journal of Neuroendocrinology **34**(4): e13110.

Daigle, T. L., L. Madisen, T. A. Hage, M. T. Valley, U. Knoblich, R. S. Larsen, M. M. Takeno, L. Huang, H. Gu, R. Larsen, M. Mills, A. Bosma-Moody, L. A. Siverts, M. Walker, L. T. Graybuck, Z. Yao, O. Fong, T. N. Nguyen, E. Garren, G. H. Lenz, M. Chavarha, J. Pendergraft, J. Harrington, K. E. Hirokawa, J. A. Harris, P. R. Nicovich, M. J. McGraw, D. R. Ollerenshaw, K. A. Smith, C. A. Baker, J. T. Ting, S. M. Sunkin, J. Lecoq, M. Z. Lin, E. S. Boyden, G. J. Murphy, N. M. da Costa, J. Waters, L. Li, B. Tasic and H. Zeng (2018). "A Suite of Transgenic Driver and Reporter Mouse Lines with Enhanced Brain-Cell-Type Targeting and Functionality." Cell **174**(2): 465-480.e422.

Dalkin, A. C., D. J. Haisenleder, G. A. Ortolano, T. R. Ellis and J. C. Marshall (1989). "The frequency of gonadotropin-releasing-hormone stimulation differentially regulates gonadotropin subunit messenger ribonucleic acid expression." Endocrinology **125**(2): 917-924.

Dam, E. W. C. M. V., F. Roelfsema, J. D. Veldhuis, F. M. Helmerhorst, M. Frölich, A. E. Meinders, H. M. J. Krans and H. Pijl (2002). "Increase in daily LH secretion in response to short-term calorie restriction in obese women with PCOS." American Journal of Physiology-Endocrinology and Metabolism **282**(4): E865-E872.

Esparza, L. A., T. Terasaka, M. A. Lawson and A. S. Kauffman (2020). "Androgen Suppresses In Vivo and In Vitro LH Pulse Secretion and Neural Kiss1 and Tac2 Gene Expression in Female Mice." Endocrinology **161**(12).

Gibson, A. G., J. Jaime, L. L. Burger and S. M. Moenter (2021). "Prenatal Androgen Treatment Does Not Alter the Firing Activity of Hypothalamic Arcuate Kisspeptin Neurons in Female Mice." eNeuro **8**(5).

Goodman, R. L., A. E. Herbison, M. N. Lehman and V. M. Navarro (2022). "Neuroendocrine control of gonadotropin-releasing hormone: Pulsatile and surge modes of secretion." Journal of Neuroendocrinology **34**(5): e13094.

Goodman, R. L., I. Holaskova, C. C. Nestor, J. M. Connors, H. J. Billings, M. Valent, M. N. Lehman and S. M. Hileman (2011). "Evidence that the Arcuate Nucleus Is an Important Site of Progesterone Negative Feedback in the Ewe." Endocrinology **152**(9): 3451-3460.

Griffond, B., A. Deray, D. Fellmann, P. Ciofi, D. Croix and C. Bugnon (1993). "Colocalization of prolactin- and dynorphin-like substances in a neuronal population of the rat lateral hypothalamus." Neurosci Lett **156**(1-2): 91-95.

Han, S. Y., G. Kane, I. Cheong and A. E. Herbison (2019). "Characterization of GnRH Pulse Generator Activity in Male Mice Using GCaMP Fiber Photometry." Endocrinology **160**(3): 557-567.

Han, S. Y., P. G. Morris, J.-C. Kim, S. Guru, M. Pardo-Navarro, S.-H. Yeo, H. J. McQuillan and A. E. Herbison (2023). "Mechanism of kisspeptin neuron synchronization for pulsatile hormone secretion in male mice." Cell Reports **42**(1): 111914.

Handelsman, D. J., E. Gibson, S. Davis, B. Golebiowski, K. A. Walters and R. Desai (2020). "Ultrasensitive Serum Estradiol Measurement by Liquid Chromatography-Mass Spectrometry in Postmenopausal Women and Mice." J Endocr Soc **4**(9): bvaa086.

Handelsman, D. J., M. Jimenez, G. K. S. Singh, J. Spaliviero, R. Desai and K. A. Walters (2015). "Measurement of Testosterone by Immunoassays and Mass Spectrometry in Mouse Serum, Testicular, and Ovarian Extracts." Endocrinology **156**(1): 400-405.

Handelsman, D. J. and L. Wartofsky (2013). "Requirement for mass spectrometry sex steroid assays in the Journal of Clinical Endocrinology and Metabolism." J Clin Endocrinol Metab **98**(10): 3971-3973.

Herbison, A. E. (2018). "The Gonadotropin-Releasing Hormone Pulse Generator." Endocrinology **159**(11): 3723-3736.

Herbison, A. E. (2021). "The dendron and episodic neuropeptide release." Journal of Neuroendocrinology **33**(11): e13024.

Jaime, J. and S. M. Moenter (2022). "GnRH Neuron Excitability and Action Potential Properties Change with Development But Are Not Affected by Prenatal Androgen Exposure." eNeuro **9**(6).

Kerbus, R. I., C. Decourt, M. A. Inglis, R. E. Campbell and G. M. Anderson (2024). "Androgen receptor actions on AgRP neurons are not a major cause of reproductive and metabolic impairments in peripubertally androgenized mice." Journal of Neuroendocrinology **n/a**(n/a): e13370.

Kumari, A. S., A. Haq, R. Jayasundaram, L. O. Abdel-Wareth, S. A. al Haija and M. Alvares (2005). "Metformin monotherapy in lean women with polycystic ovary syndrome." Reproductive BioMedicine Online **10**(1): 100-104.

Lei, L., L. Ding, J. Su, M. Liu, Q. Shi, J. Zhou, H. Sun and G. Yan (2017). "Attenuated expression of MTR in both prenatally androgenized mice and women with the hyperandrogenic phenotype of PCOS." PLoS One **12**(12): e0187427.

Leipheimer, R. E., A. Bona-Gallo and R. V. Gallo (1984). "The influence of progesterone and estradiol on the acute changes in pulsatile luteinizing hormone release induced by ovariectomy on diestrus day 1 in the rat." Endocrinology **114**(5): 1605-1612.

Lerner, T. N., C. Shilyansky, T. J. Davidson, K. E. Evans, K. T. Beier, K. A. Zalocusky, A. K. Crow, R. C. Malenka, L. Luo, R. Tomer and K. Deisseroth (2015). "Intact-Brain Analyses Reveal Distinct Information Carried by SNc Dopamine Subcircuits." Cell **162**(3): 635-647.

Liu, X., S.-H. Yeo, H. J. McQuillan, M. K. Herde, S. Hessler, I. Cheong, R. Porteous and A. E. Herbison (2021). "Highly redundant neuropeptide volume co-transmission underlying episodic activation of the GnRH neuron dendron." eLife **10**: e62455.

Lizneva, D., L. Suturina, W. Walker, S. Brakta, L. Gavrilova-Jordan and R. Azziz (2016). "Criteria, prevalence, and phenotypes of polycystic ovary syndrome." Fertility and Sterility **106**(1): 6-15.

McCarthy, E. A., D. Dischino, C. Maguire, S. Leon, R. Talbi, E. Cheung, C. D. Schteingart, P. J. M. Rivière, S. D. Reed, R. A. Steiner and V. M. Navarro (2021). "Inhibiting Kiss1 Neurons With Kappa Opioid Receptor Agonists to Treat Polycystic Ovary Syndrome and Vasomotor Symptoms." The Journal of Clinical Endocrinology & Metabolism **107**(1): e328-e347.

McQuillan, H. J., J. Clarkson, A. Kauff, S. Y. Han, S. H. Yip, I. Cheong, R. Porteous, A. K. Heather and A. E. Herbison (2022). "Definition of the estrogen negative feedback pathway controlling the GnRH pulse generator in female mice." Nature Communications **13**(1): 7433.

McQuillan, H. J., J. Clarkson, A. Kauff, S. Y. Han, S. H. Yip, I. Cheong, R. Porteous, A. K. Heather and A. E. Herbison (2022). "Definition of the estrogen negative feedback pathway controlling the GnRH pulse generator in female mice." Nat Commun **13**(1): 7433.

McQuillan, H. J., S. Y. Han, I. Cheong and A. E. Herbison (2019). "GnRH Pulse Generator Activity Across the Estrous Cycle of Female Mice." Endocrinology **160**(6): 1480-1491.

Moore, A. M., D. B. Lohr, L. M. Coolen and M. N. Lehman (2021). "Prenatal Androgen Exposure Alters KNDy Neurons and Their Afferent Network in a Model of Polycystic Ovarian Syndrome." Endocrinology **162**(11).

Moore, A. M., M. Prescott and R. E. Campbell (2013). "Estradiol Negative and Positive Feedback in a Prenatal Androgen-Induced Mouse Model of Polycystic Ovarian Syndrome." Endocrinology **154**(2): 796-806.

Moore, A. M., M. Prescott, C. J. Marshall, S. H. Yip and R. E. Campbell (2015). "Enhancement of a robust arcuate GABAergic input to gonadotropin-releasing hormone neurons in a model of polycystic ovarian syndrome." Proc Natl Acad Sci U S A **112**(2): 596-601.

Morales, A., G. Laughlin, T. Bützow, H. Maheshwari, G. Baumann and S. Yen (1996). "Insulin, somatotropic, and luteinizing hormone axes in lean and obese women with polycystic ovary syndrome: common and distinct features." The Journal of Clinical Endocrinology & Metabolism **81**(8): 2854-2864.

Morales, A. J., G. A. Laughlin, T. Bützow, H. Maheshwari, G. Baumann and S. S. Yen (1996). "Insulin, somatotropic, and luteinizing hormone axes in lean and obese women with polycystic ovary syndrome: common and distinct features." The Journal of Clinical Endocrinology & Metabolism **81**(8): 2854-2864.

Morris, P. G. and A. E. Herbison (2023). "Mechanism of Arcuate Kisspeptin Neuron Synchronization in Acute Brain Slices From Female Mice." Endocrinology **164**(12).

Navarro, V. M., M. L. Gottsch, C. Chavkin, H. Okamura, D. K. Clifton and R. A. Steiner (2009). "Regulation of gonadotropin-releasing hormone secretion by kisspeptin/dynorphin/neurokinin B neurons in the arcuate nucleus of the mouse." J Neurosci **29**(38): 11859-11866.

Nestler, J. E. and D. J. Jakubowicz (1997). "Lean women with polycystic ovary syndrome respond to insulin reduction with decreases in ovarian P450c17 alpha activity and serum androgens." J Clin Endocrinol Metab **82**(12): 4075-4079.

Osuka, S., A. Iwase, T. Nakahara, M. Kondo, A. Saito, Bayasula, T. Nakamura, S. Takikawa, M. Goto, T. Kotani and F. Kikkawa (2016). "Kisspeptin in the Hypothalamus of 2 Rat Models of Polycystic Ovary Syndrome." Endocrinology **158**(2): 367-377.

Pastor, C. L., M. L. Griffin-Korf, J. A. Aloi, W. S. Evans and J. C. Marshall (1998). "Polycystic Ovary Syndrome: Evidence for Reduced Sensitivity of the Gonadotropin-Releasing Hormone Pulse Generator to Inhibition by Estradiol and Progesterone1." The Journal of Clinical Endocrinology & Metabolism **83**(2): 582-590.

Patel, K., M. S. Coffler, M. H. Dahan, R. Y. Yoo, M. A. Lawson, P. J. Malcom and R. J. Chang (2003). "Increased luteinizing hormone secretion in women with polycystic ovary syndrome is unaltered by prolonged insulin infusion." J Clin Endocrinol Metab **88**(11): 5456-5461.

Phylactou, M., S. A. Clarke, B. Patel, C. Baggaley, C. N. Jayasena, T. W. Kelsey, A. N. Comninos, W. S. Dhillo and A. Abbara (2021). "Clinical and biochemical discriminants between functional hypothalamic amenorrhoea (FHA) and polycystic ovary syndrome (PCOS)." Clinical Endocrinology **95**(2): 239-252.

Porteous, R., P. Haden, E. C. R. Hackwell, A. Singline, M. K. Herde, R. Desai, D. J. Handelsman, D. R. Grattan and A. E. Herbison (2021). "Reformulation of PULSAR for Analysis of Pulsatile LH Secretion and a Revised Model of Estrogen-Negative Feedback in Mice." Endocrinology **162**(11).

Qiu, J., C. C. Nestor, C. Zhang, S. L. Padilla, R. D. Palmiter, M. J. Kelly and O. K. Rønnekleiv (2016). "High-frequency stimulation-induced peptide release synchronizes arcuate kisspeptin neurons and excites GnRH neurons." eLife **5**: e16246.

Risal, S., M. Manti, H. Lu, R. Fornes, H. Larsson, A. Benrick, Q. Deng, C. E. Cesta, M. A. Rosenqvist and E. Stener-Victorin (2021). "Prenatal androgen exposure causes a sexually dimorphic transgenerational increase in offspring susceptibility to anxiety disorders." Translational Psychiatry **11**(1): 45.

Rodriguez Paris, V. and M. J. Bertoldo (2019). "The Mechanism of Androgen Actions in PCOS Etiology." Medical Sciences **7**(9): 89.

Roland, A. V. and S. M. Moenter (2011). "Prenatal androgenization of female mice programs an increase in firing activity of gonadotropin-releasing hormone (GnRH) neurons that is reversed by metformin treatment in adulthood." Endocrinology **152**(2): 618-628.

Ruddenklau, A. and R. E. Campbell (2019). "Neuroendocrine Impairments of Polycystic Ovary Syndrome." Endocrinology **160**(10): 2230-2242.

Silva, M. S., M. Prescott and R. E. Campbell (2018). "Ontogeny and reversal of brain circuit abnormalities in a preclinical model of PCOS." JCI Insight **3**(7).

Silva, M. S. B., E. Desroziers, S. Hessler, M. Prescott, C. Coyle, A. E. Herbison and R. E. Campbell (2019). "Activation of arcuate nucleus GABA neurons promotes luteinizing hormone secretion and reproductive dysfunction: Implications for polycystic ovary syndrome." EBioMedicine **44**: 582-596.

Singh, J., C. O'Neill and D. J. Handelsman (1995). "Induction of spermatogenesis by androgens in gonadotropin-deficient (hpg) mice." Endocrinology **136**(12): 5311-5321.

Stener-Victorin, E., V. Padmanabhan, K. A. Walters, R. E. Campbell, A. Benrick, P. Giacobini, D. A. Dumesic and D. H. Abbott (2020). "Animal Models to Understand the Etiology and Pathophysiology of Polycystic Ovary Syndrome." Endocr Rev **41**(4).

Steyn, F. J., Y. Wan, J. Clarkson, J. D. Veldhuis, A. E. Herbison and C. Chen (2013). "Development of a methodology for and assessment of pulsatile luteinizing hormone secretion in juvenile and adult male mice." Endocrinology **154**(12): 4939-4945.

Sullivan, S. D. and S. M. Moenter (2004). "Prenatal androgens alter GABAergic drive to gonadotropin-releasing hormone neurons: implications for a common fertility disorder." Proc Natl Acad Sci U S A **101**(18): 7129-7134.

Taylor, A. E., B. McCourt, K. A. Martin, E. J. Anderson, J. M. Adams, D. Schoenfeld and J. E. Hall (1997). "Determinants of Abnormal Gonadotropin Secretion in Clinically Defined Women with Polycystic Ovary Syndrome." The Journal of Clinical Endocrinology & Metabolism **82**(7): 2248-2256.

The Rotterdam ESHRE/ASRM-sponsored PCOS consensus workshop group (2004). "Revised 2003 consensus on diagnostic criteria and long-term health risks related to polycystic ovary syndrome (PCOS)." Human Reproduction **19**(1): 41-47.

Toosy, S., R. Sodi and J. M. Pappachan (2018). "Lean polycystic ovary syndrome (PCOS): an evidence-based practical approach." J Diabetes Metab Disord **17**(2): 277-285.

van Houten, E. L. A. F., P. Kramer, A. McLuskey, B. Karels, A. P. N. Themmen and J. A. Visser (2012). "Reproductive and Metabolic Phenotype of a Mouse Model of PCOS." Endocrinology **153**(6): 2861-2869.

Vas, S., E. Wall, Z. Zhou, L. Kalmar, S. Y. Han and A. E. Herbison (2024). "Long-term recordings of arcuate nucleus kisspeptin neurons across the mouse estrous cycle." Endocrinology.

Waldstreicher, J., N. F. Santoro, J. E. Hall, M. Filicori and W. F. Crowley, Jr. (1988). "Hyperfunction of the hypothalamic-pituitary axis in women with polycystic ovarian disease: indirect evidence for partial gonadotroph desensitization." J Clin Endocrinol Metab **66**(1): 165-172.

Wall, E. G., R. Desai, Z. Khant Aung, S. H. Yeo, D. R. Grattan, D. J. Handelsman and A. E. Herbison (2023). "Unexpected Plasma Gonadal Steroid and Prolactin Levels Across the Mouse Estrous Cycle." Endocrinology **164**(6).

Walters, K. A., R. B. Gilchrist, W. L. Ledger, H. J. Teede, D. J. Handelsman and R. E. Campbell (2018). "New Perspectives on the Pathogenesis of PCOS: Neuroendocrine Origins." Trends in Endocrinology & Metabolism **29**(12): 841-852.

Wang, L., W. Guo, X. Shen, S. Yeo, H. Long, Z. Wang, Q. Lyu, A. E. Herbison and Y. Kuang (2020). "Different dendritic domains of the GnRH neuron underlie the pulse and surge modes of GnRH secretion in female mice." eLife **9**: e53945.

Watanabe, Y., L. Fisher, R. E. Campbell and C. L. Jasoni (2023). "Defining potential targets of prenatal androgen excess: Expression analysis of androgen receptor on hypothalamic neurons in the fetal female mouse brain." Journal of Neuroendocrinology **35**(6): e13302.

Wierman, M. E., R. J. Auchus, D. J. Haisenleder, J. E. Hall, D. Handelsman, S. Hankinson, W. Rosner, R. J. Singh, P. M. Sluss and F. Z. Stanczyk (2014). "Editorial: The new instructions to authors for the reporting of steroid hormone measurements." J Clin Endocrinol Metab **99**(12): 4375.

Wildt, L., A. Häusler, G. Marshall, J. S. Hutchison, T. M. Plant, P. E. Belchetz and E. Knobil (1981). "Frequency and amplitude of gonadotropin-releasing hormone stimulation and gonadotropin secretion in the rhesus monkey." Endocrinology **109**(2): 376-385.

Wong, R., D. Ray and D. A. Kendall (2012). "Progesterone pharmacokinetics in the mouse: implications for potential stroke therapy." Journal of Pharmacy and Pharmacology **64**(11): 1614-1620.

Yan, X., C. Yuan, N. Zhao, Y. Cui and J. Liu (2014). "Prenatal androgen excess enhances stimulation of the GNRH pulse in pubertal female rats." Journal of Endocrinology **222**(1): 73-85.

Yeo, S. H., V. Kyle, P. G. Morris, S. Jackman, L. C. Sinnett-Smith, M. Schacker, C. Chen and W. H. Colledge (2016). "Visualisation of Kiss1 Neurone Distribution Using a Kiss1-CRE Transgenic Mouse." J Neuroendocrinol **28**(11).

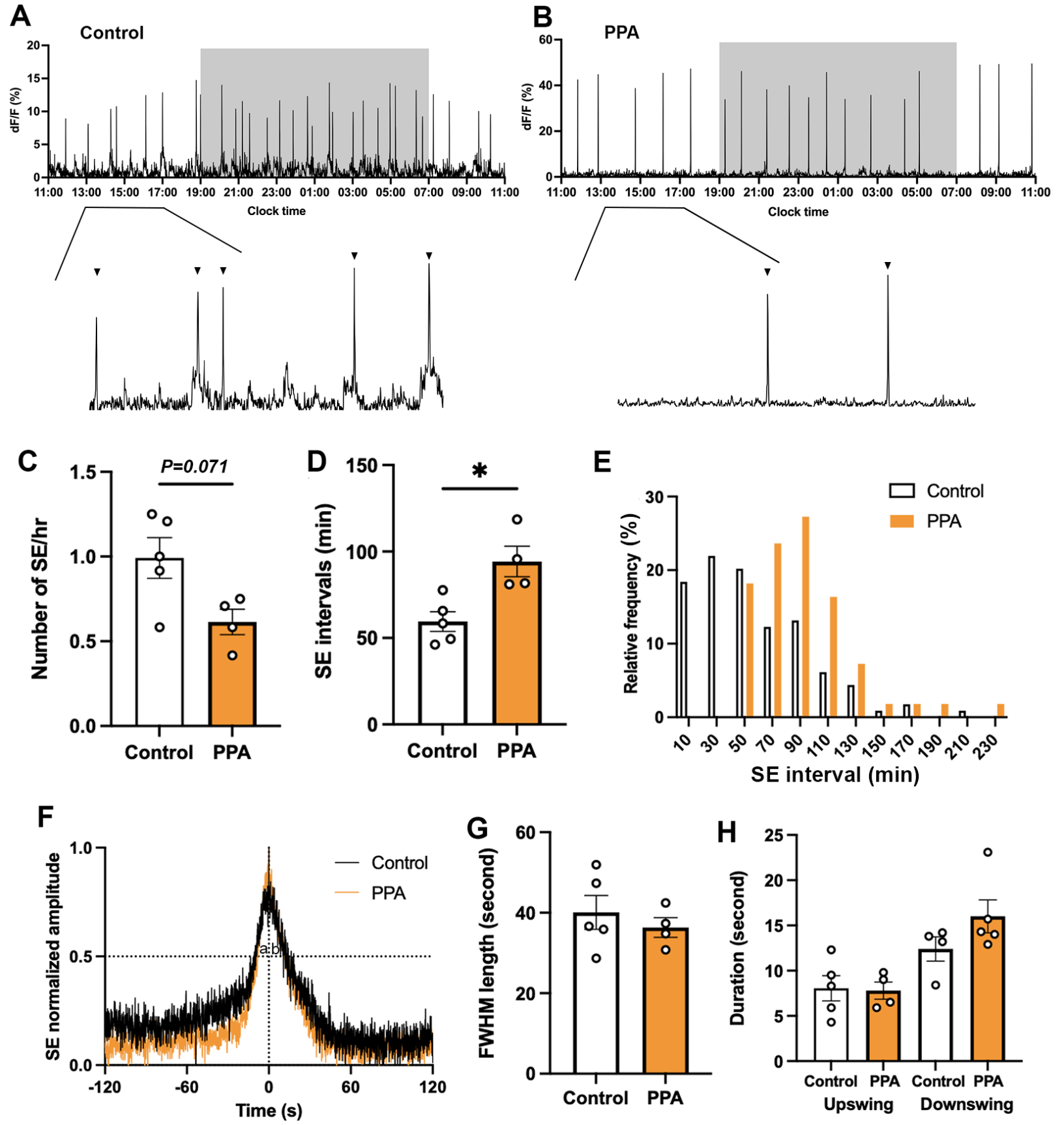
A
Control
dF/F (%)
Clock time
B
PPA
dF/F (%)
Clock time
C
P=0.071
Number of SE/hr
Control
PPA
D
*
SE intervals (min)
Control
PPA
E
Control
PPA
Relative frequency (%)
SE interval (min)
F
Control
PPA
SE normalized amplitude
Time (s)
G
FWHM length (second)
Control
PPA
H
Duration (second)
Control
PPA
Control
PPA
Upswing
Downswing

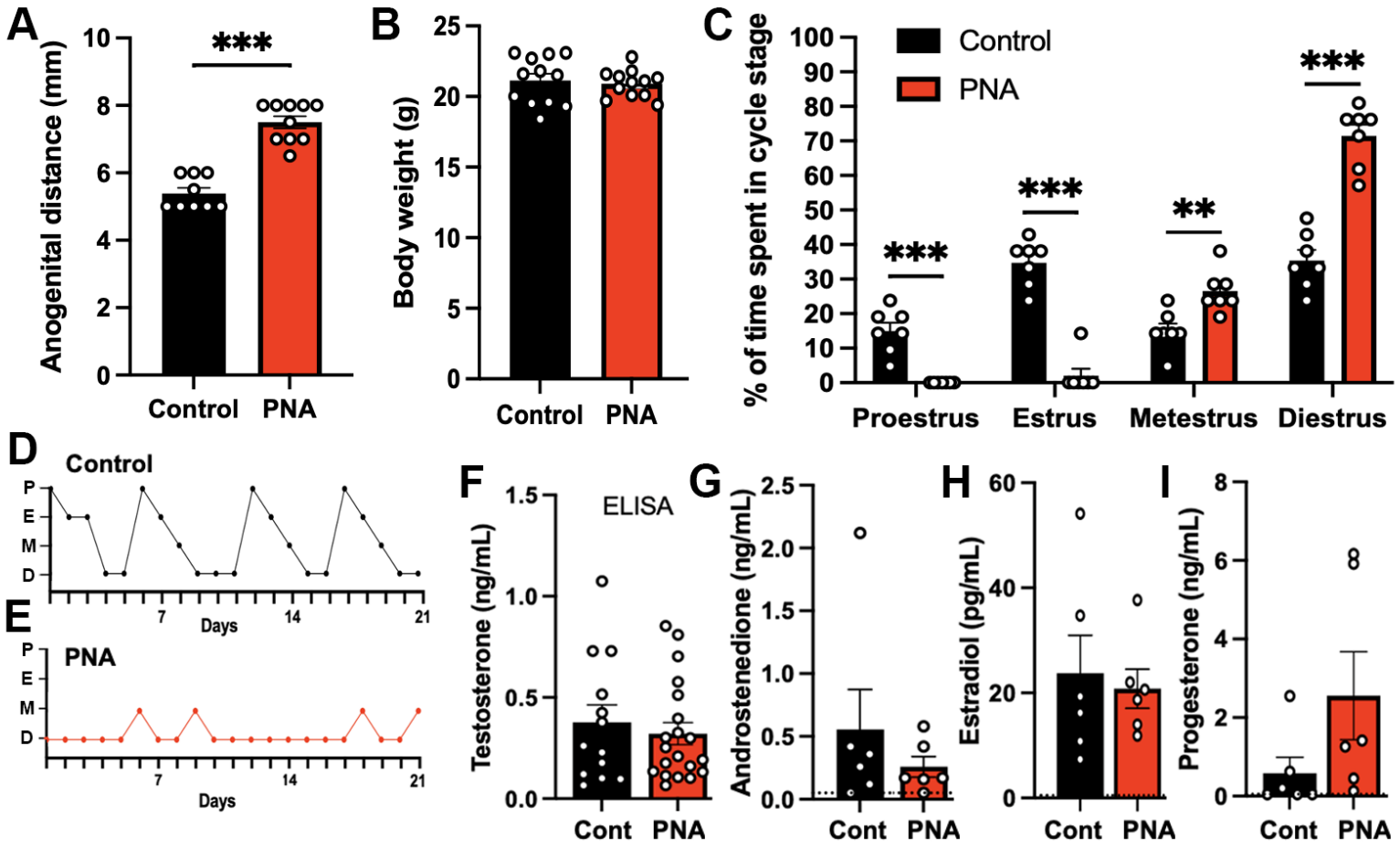
A
Anogenital distance (mm)
***
Control
PNA
B
Body weight (g)
Control
PNA
C
% of time spent in cycle stage
Control
PNA
***
***
**
***
Proestrus
Estrus
Metestrus
Diestrus
D
Control
P
E
M
D
7
14
21
Days
E
PNA
P
E
M
D
7
14
21
Days
F
ELISA
Testosterone (ng/mL)
Cont
PNA
G
Androstenedione (ng/mL)
Cont
PNA
H
Estradiol (pg/mL)
Cont
PNA
I
Progesterone (ng/mL)
Cont
PNA

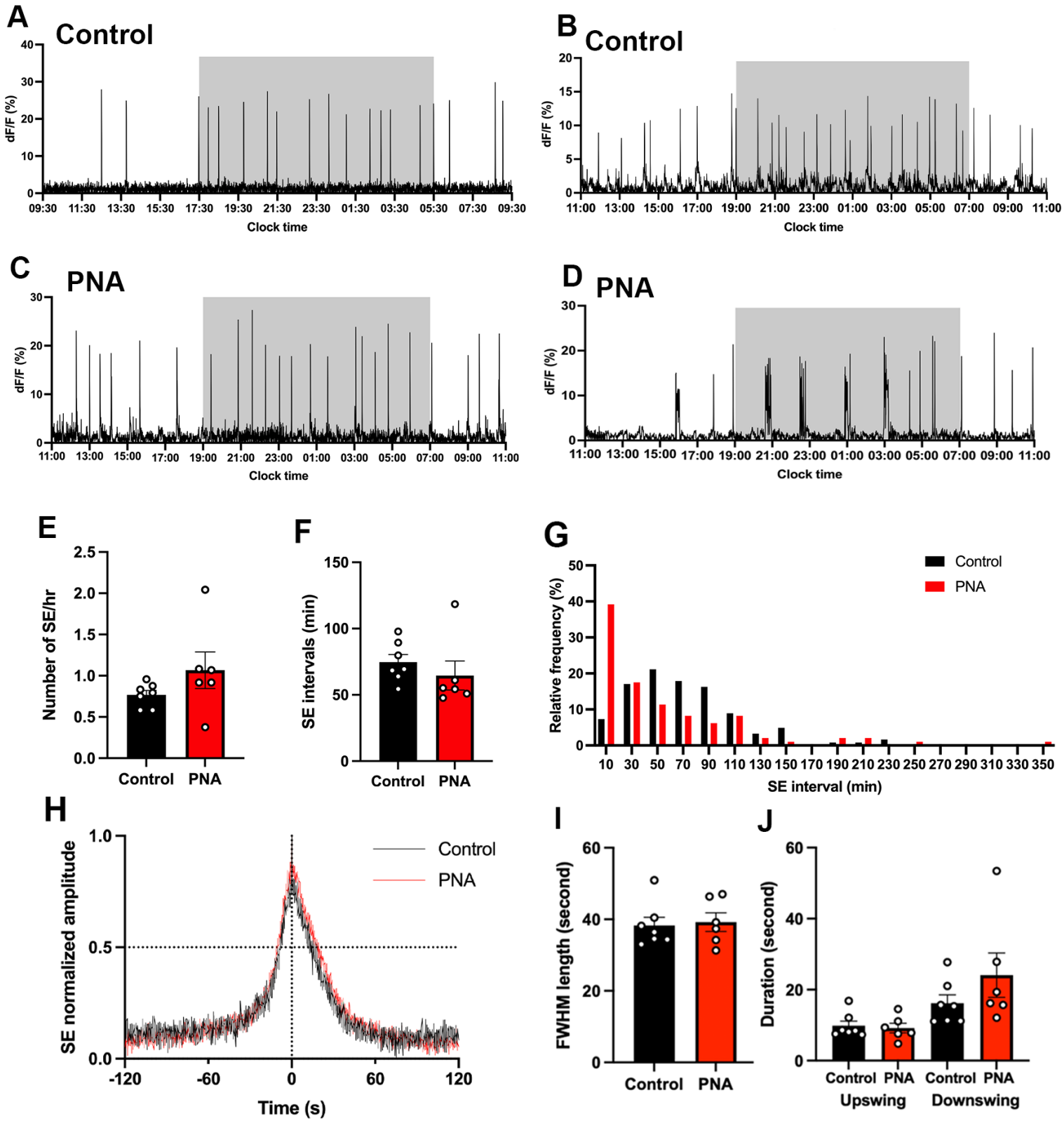
A
Control
dF/F (%)
Clock time
B
Control
dF/F (%)
Clock time
C
PNA
dF/F (%)
Clock time
D
PNA
dF/F (%)
Clock time
E
Number of SE/hr
Control
PNA
F
SE intervals (min)
Control
PNA
G
Control
PNA
Relative frequency (%)
SE interval (min)
H
Control
PNA
SE normalized amplitude
Time (s)
I
FWHM length (second)
Control
PNA
J
Duration (second)
Control
PNA
Control
PNA
Upswing
Downswing

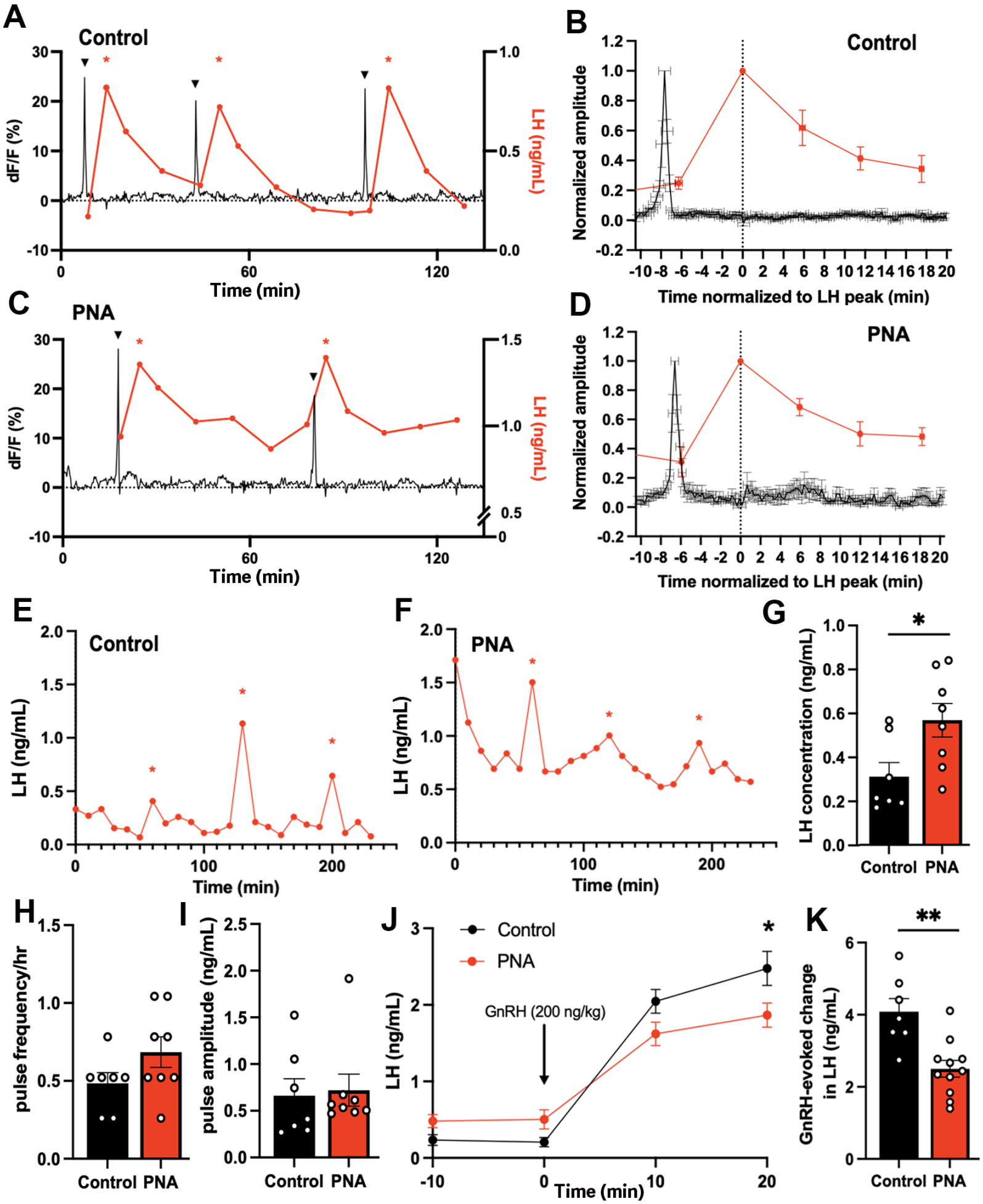
A
Control
dF/F (%)
LH (ng/mL)
Time (min)
B
Control
Normalized amplitude
Time normalized to LH peak (min)
C
PNA
dF/F (%)
LH (ng/mL)
Time (min)
D
PNA
Normalized amplitude
Time normalized to LH peak (min)
E
Control
LH (ng/mL)
Time (min)
F
PNA
LH (ng/mL)
Time (min)
G
LH concentration (ng/mL)
Control
PNA
H
pulse frequency/hr
Control
PNA
I
pulse amplitude (ng/mL)
Control
PNA
J
Control
PNA
GnRH (200 ng/kg)
LH (ng/mL)
Time (min)
K
GnRH-evoked change in LH (ng/mL)
Control
PNA

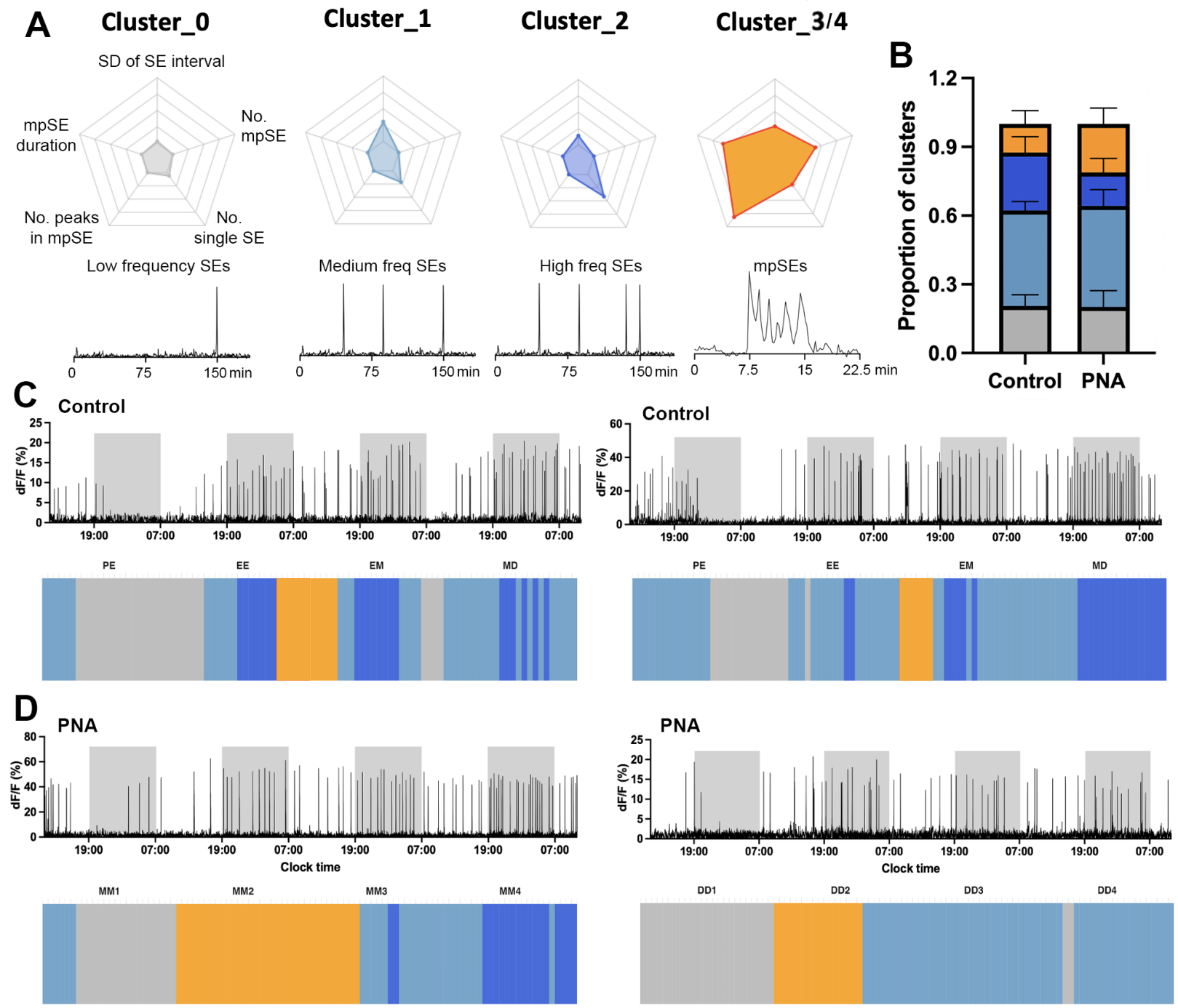
A
Cluster_0
Cluster_1
Cluster_2
Cluster_3/4
SD of SE interval
mpSE duration
No. mpSE
No. peaks in mpSE
No. single SE
Low frequency SEs
Medium freq SEs
High freq SEs
mpSEs
0
75
150 min
7.5
15
22.5 min
B
Proportion of clusters
1.2
0.9
0.6
0.3
0.0
Control
PNA
C
Control
dF/F (%)
19:00
07:00
PE
EE
EM
MD
D
PNA
Clock time
MM1
MM2
MM3
MM4
DD1
DD2
DD3
DD4

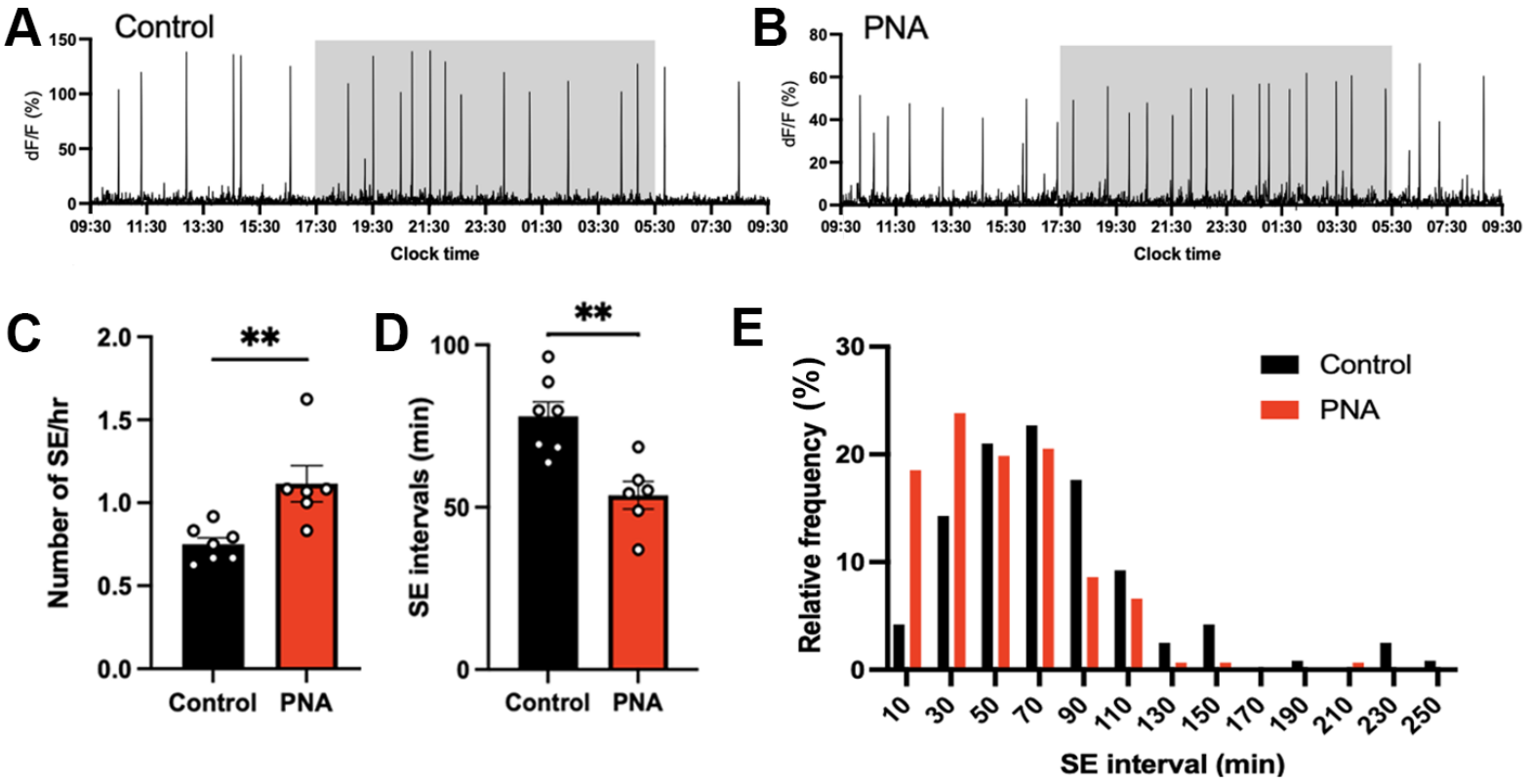
A
Control
dF/F (%)
150
100
50
0
09:30
11:30
13:30
15:30
17:30
19:30
21:30
23:30
01:30
03:30
05:30
07:30
09:30
Clock time
B
PNA
dF/F (%)
80
60
40
20
0
09:30
11:30
13:30
15:30
17:30
19:30
21:30
23:30
01:30
03:30
05:30
07:30
09:30
Clock time
C
**
Number of SE/hr
2.0
1.5
1.0
0.5
0.0
Control
PNA
D
**
SE intervals (min)
100
50
0
Control
PNA
E
Relative frequency (%)
30
20
10
0
Control
PNA
10
30
50
70
90
110
130
150
170
190
210
230
250
SE interval (min)

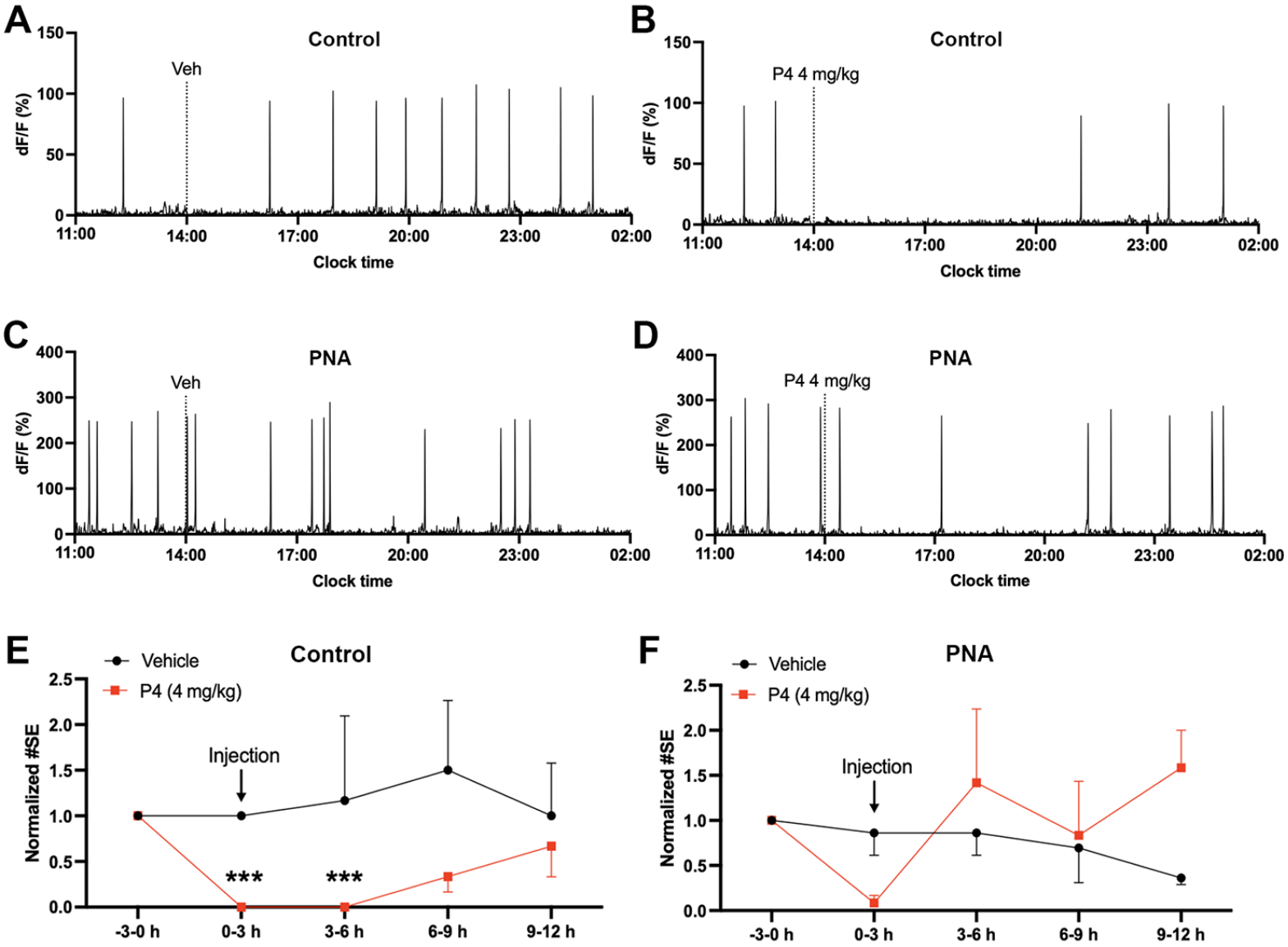
A
Control
Veh
dF/F (%)
150
100
50
0
11:00
14:00
17:00
20:00
23:00
02:00
Clock time
B
Control
P4 4 mg/kg
dF/F (%)
150
100
50
0
11:00
14:00
17:00
20:00
23:00
02:00
Clock time
C
PNA
Veh
dF/F (%)
400
300
200
100
0
11:00
14:00
17:00
20:00
23:00
02:00
Clock time
D
PNA
P4 4 mg/kg
dF/F (%)
400
300
200
100
0
11:00
14:00
17:00
20:00
23:00
02:00
Clock time
E
Control
Vehicle
P4 (4 mg/kg)
Injection
Normalized #SE
2.5
2.0
1.5
1.0
0.5
0.0
***
***
-3-0 h
0-3 h
3-6 h
6-9 h
9-12 h
F
PNA
Vehicle
P4 (4 mg/kg)
Injection
Normalized #SE
2.5
2.0
1.5
1.0
0.5
0.0
-3-0 h
0-3 h
3-6 h
6-9 h
9-12 h

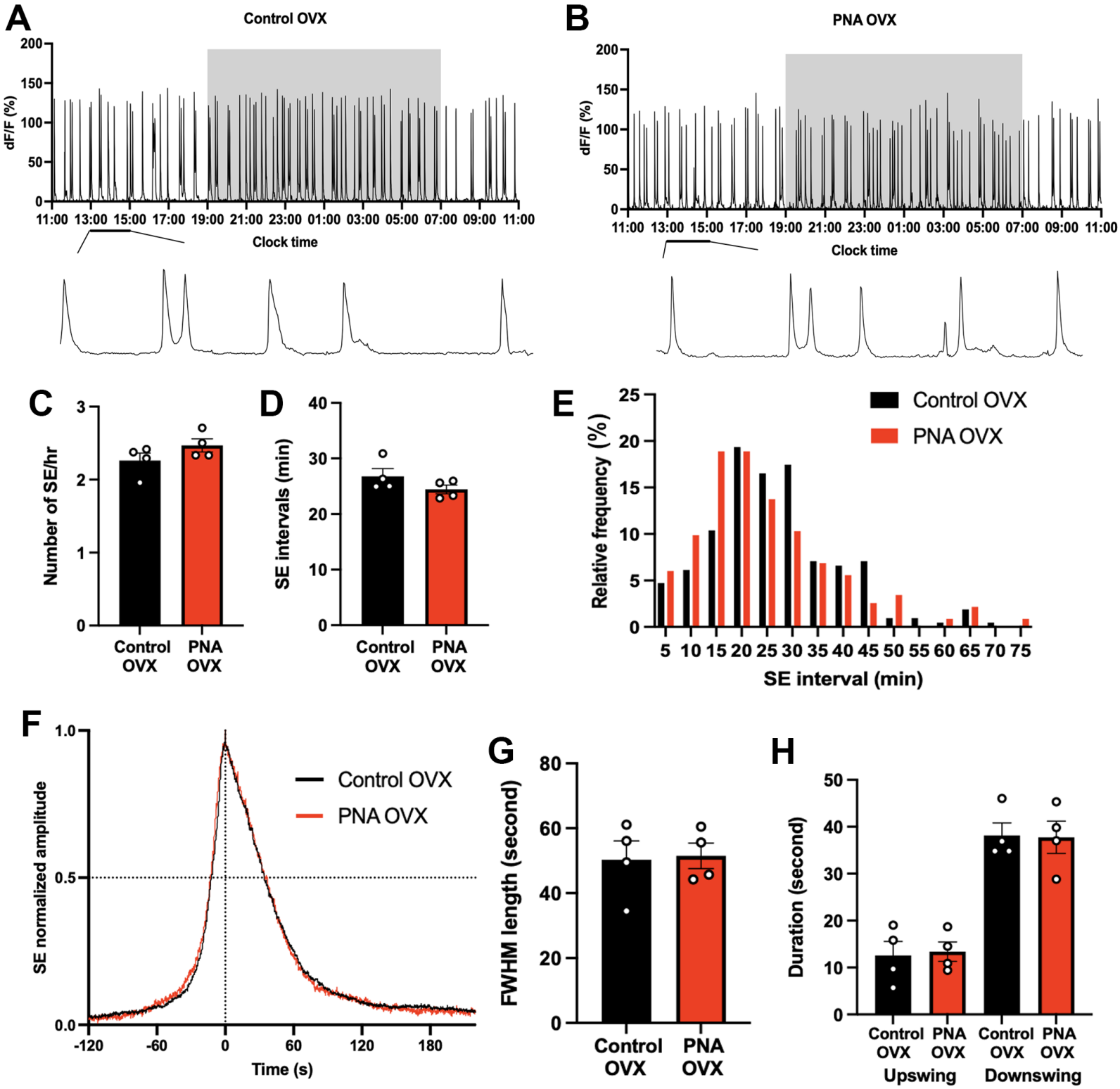
A
Control OVX
dF/F (%)
200
150
100
50
0
11:00 13:00 15:00 17:00 19:00 21:00 23:00 01:00 03:00 05:00 07:00 09:00 11:00
Clock time
B
PNA OVX
dF/F (%)
200
150
100
50
0
11:00 13:00 15:00 17:00 19:00 21:00 23:00 01:00 03:00 05:00 07:00 09:00 11:00
Clock time
C
Number of SE/hr
3
2
1
0
Control OVX
PNA OVX
D
SE intervals (min)
40
30
20
10
0
Control OVX
PNA OVX
E
Relative frequency (%)
25
20
15
10
5
0
Control OVX
PNA OVX
5 10 15 20 25 30 35 40 45 50 55 60 65 70 75
SE interval (min)
F
SE normalized amplitude
1.0
0.5
0.0
Control OVX
PNA OVX
-120 -60 0 60 120 180
Time (s)
G
FWHM length (second)
80
60
40
20
0
Control OVX
PNA OVX
H
Duration (second)
50
40
30
20
10
0
Control OVX
PNA OVX
Control OVX
PNA OVX
Upswing
Downswing